1

Low-*k* Materials: Recent Advances

Geraud Dubois and Willi Volksen

Hybrid Polymeric Materials Group, IBM Almaden Research Center, San Jose, California, USA

COPYRIGHTED MATERIAL

1.1 Introduction

From a historical point of view, the search for new low-*k* and ultra-low-*k* materials has always been dictated by industrial needs, resulting in a strong connection between fundamental research and technology. Although a variety of potential candidates has been reported in the literature during the past decade, integration is the deciding factor driving the selection of the most promising materials for a given technology node [1]. For instance, the industry flirted briefly with organic polymers [2–7]. Besides the anticipated thermal stability challenges, this class of materials, known to be tough and crack-resistant, had other issues, such as softness, large coefficient of thermal expansions (CTE) and delamination. While most of these problems were mitigated by material reengineering and chip redesign, solutions occurred too late, relegating the organic polymers to possible hybrid build applications [8]. For the new low-*k* materials, it was expected that their electrical and mechanical properties would be comparable to those of silicon dioxide [9, 10], the insulating material of reference for the quite conservative semiconductor industry. Chemical modification of the silicon network, first by introduction of fluorine and eventually by the addition of carbon, was then adopted as the lower risk path to introducing low-*k* materials in the back-end-of-the-line (BEOL) [1]. At that time, silicates and

Advanced Interconnects for ULSI Technology, First Edition. Edited by Mikhail R. Baklanov, Paul S. Ho and Ehrenfried Zschech.
© 2012 John Wiley & Sons, Ltd. Published 2012 by John Wiley & Sons, Ltd.

organosilicates emerged as the dominant candidates. They can be deposited by both spin-on and chemical vapor deposition (CVD) processes. However, the final thin-film properties are in large part dictated by the chemical structure of the deposited film, a result of both the precursor or resin chemistry and the deposition process. From before 1997 until now (Figure 1.1), plasma-enhanced chemical vapor deposition (PECVD) has been the method of choice for depositing silicon dioxide (SiO_2), fluorine-doped oxides (F-SiO_2), carbon-doped oxides (SiCOH: elementally descriptive but not representing the stoichiometry) and porous carbon-doped oxides (p-SiCOH). As illustrated in Figure 1.1, PECVD SiCOH materials were successfully implemented in IBM microprocessors: at the 90 nm ($k = 3.0$) and 65 nm ($k = 2.7$) technology nodes in 2004 and 2006, respectively. PECVD materials containing additional porosity (p-SiCOH) appeared for the first time in high-volume manufacturing in 2008 (Figure 1.1).

Interestingly, the real IBM technology node/dielectric constant relationship differs significantly from the targets proposed by the NTRS in 1997. This shows the danger of predicting dielectric targets based solely on engineering designs when new materials are not readily available. The challenges in designing dielectric insulators that meet all the BEOL requirements (electrical, thermal and mechanical) have been the source of many publications over the last 15 years [1]. Among them, many excellent reviews have been published, addressing the different aspects of these dielectric materials: physical properties [7, 11–13], integration requirements and challenges [14, 15], characterization [9, 16–19] and chemistry [1]. For advanced and future technologies, the addition of porosity at levels necessary to obtain dielectric constants of 2.4 and beyond has exacerbated already known integration issues [14]. In particular, the processing induced damage and the decrease in material mechanical properties present serious concerns for the reliability of these advanced structures. In this chapter, we will first define the main integration challenges currently encountered. Then we will discuss proposed solutions to these issues by both alternative processing approaches and development of advanced novel materials.

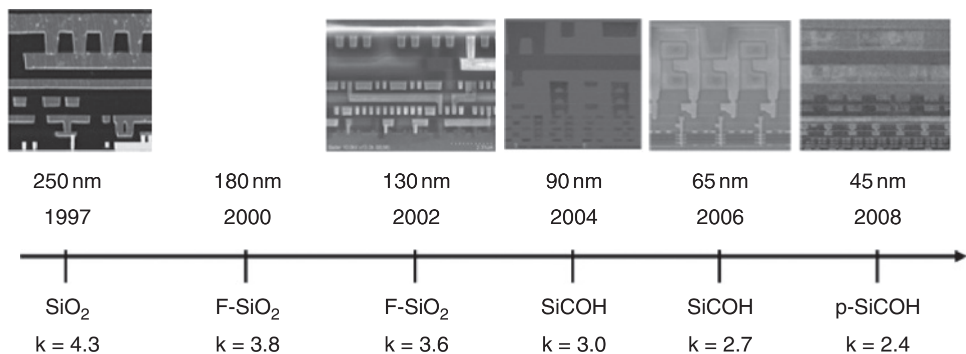

Figure 1.1 *Timeline for IBM volume manufacturing of CMOS microprocessors from 1997 to 2008*

1.2 Integration Challenges

The design of low-*k* dielectric materials with the requisite properties needed for implementation into modern semiconductor manufacturing processes is an extremely challenging task. In large part, this is a consequence of trying to adapt SiO_2-based processes to carbon containing low-*k* dielectric materials with or without additional porosity. Whereas the introduction of carbon into the inorganic network can provide an initial lowering of the dielectric constant, addition of porosity is required to achieve ultra-low-*k* (ULK) performance.

The introduction of carbon and the addition of porosity serve merely in the process of lowering the dielectric constant and nothing more. However, along with this single beneficial attribute come two major drawbacks. Firstly, the increased, accessible surface area of the porous network constitutes a new weakness with regard to plasma-induced damage and wet chemistry processes. Secondly, the decrease in network connectivity as compared to silica and the reduction of density strongly impact the dielectric insulator mechanical properties.

The comparative relationship of the interlayer-dielectric (ILD) mechanical properties and ILD process-induced damage as a function of porosity and materials chemistry is presented in Figure 1.2. It should be mentioned that these trends are qualitative in nature only. Nevertheless, they clearly demonstrate the ever-growing challenges in successfully building advanced semiconductor structures with increased performance and good reliability.

The process-induced damage is primarily reflected in deterioration of the dielectric constant, leakage current and breakdown voltage. It can also affect the mechanical properties of the integrated structure, although these are more dependent on the initial materials characteristics. The Young's modulus (*E*), hardness (*H*) and adhesive/cohesive fracture

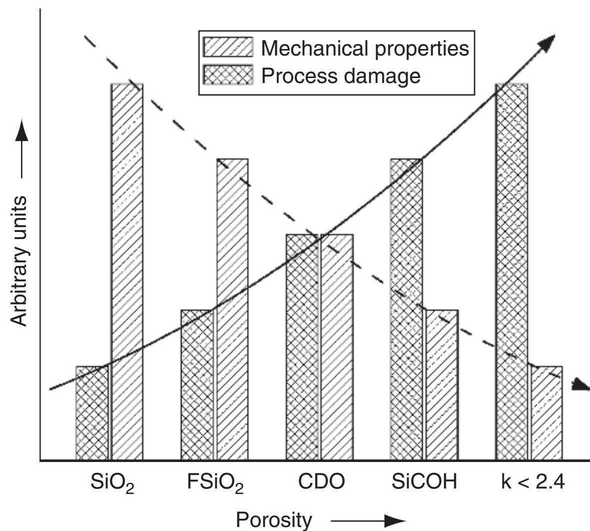

Figure 1.2 *Comparative relationship of ILD mechanical properties and ILD process-induced damage as a function of porosity and materials chemistry*

resistance (G) of future ultra-low-k materials have reached a level where the mechanical integrity of the device is of major concern.

1.2.1 Process-Induced Damage

In order to identify and better visualize key integration issues as encountered in a typical dual damascene (DD) 'via-first' approach [20], the reader is referred to Figure 1.3. Here the critical integration areas are arranged in alphabetical order, following a sequence that might be encountered in a typical process flow. For the sake of simplification, the integration processes are further broken down into pre- and post-metallization steps.

In the pre-metallization portion of the 'via-first' integration approach, the first problem areas encountered are a result of the introduction of new interfaces. As with many interfaces, adhesion at such boundary layers is of tremendous importance. The first interface results from the ILD deposition on a capping layer, which serves to protect the underlying copper metal (see Figure 1.3 (a)). Capping layers composed of SiN_x, SiC_xN_y and SiC_x are commonly employed and present surface chemistries considerably different from those based on SiO_x [21–25]. Coupled with the fact that adhesive properties scale inversely with porosity [26, 27], this combination may lead to severe delamination during chemical–mechanical polishing (CMP) and chip–package interaction (CPI). To prevent such a catastrophic failure, the capping layer surfaces are modified by plasma treatment

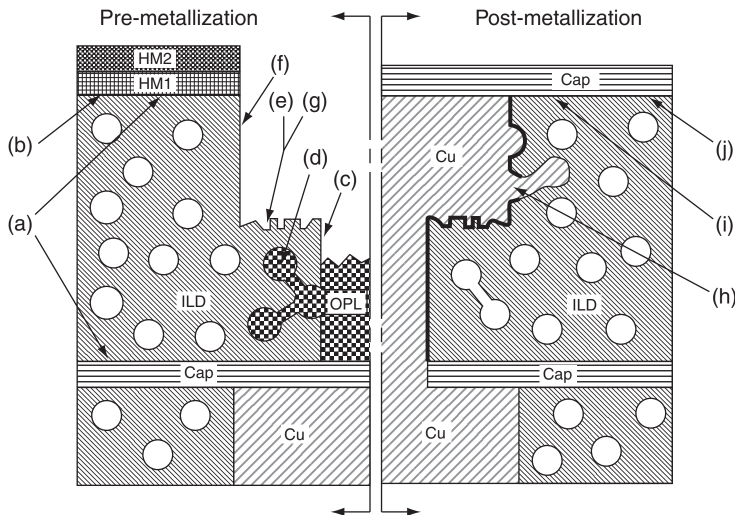

Figure 1.3 Simple, two-layer dual-damascene cross-section illustrating various process-related problem areas before and after metallization: (a) adhesion failure, (b) ILD plasma damage, (c) sidewall ILD damage from via-etch and PR strip, (d) OPL penetration during via-fill, (e) LBR and pitting from uneven etch front, (f) sidewall ILD damage from line etch and PR strip, (g) exacerbated LBR and pitting due to cap-open, (h) discontinuous barrier layer due to large, interconnected pores, (i) ILD damage from CMP, (j) Cu pre-clean/cap deposition plasma damage

or, as in the case of CVD-deposited porous ILDs, by employing a gradient layer at the interface [28]. Dense ILD is deposited at the immediate cap/ILD interface, ensuring good adhesion by eliminating the effect of porosity and then continuously increasing the porosity of the ILD until the target *k* is reached. Other new interfaces are created during hardmask deposition, which usually consists of two layers, HM1 and HM2, *vide infra* [29–31]. The function of the hardmask is to prevent direct contact of the photoresist (PR) with the ILD in order to eliminate the absorption of basic species, such as atmospheric amines, by the highly porous ILD, which leads to poisoning of the highly sensitive chemically amplified photoresists [32–34]. An additional function of the hardmask is to allow for PR rework.

The PR rework process typically involves the use of O_2 plasmas, requiring the use of SiO_2 as a hardmask (HM2). However, since SiO_2 plasma deposition processes severely damage porous, low-*k* ILDs, an intermediate layer (HM1) is deposited prior to the SiO_2 layer. For HM1, plasma deposition conditions are selected that are considerably less damaging to the porous ILD, yet provide sufficient adhesion during ensuing CMP processes (Figure 1.3 (a) and (b)) [35].

Next, via-structures are lithographically patterned and etched into the porous ILD employing C_xF_y-based plasmas [36]. These etch processes, initially developed for SiO_2 or other dense materials, tend to damage the via-sidewalls (Figure 1.3 (c)) [37–39]. By carefully balancing the polymerization and etch reactions of the plasma process, less damaging etch processes are possible. However, plasma damage to the via-sidewall is not limited to the etch step. In fact, the majority of the sidewall damage can be attributed to the strip (ash) of the remaining photoresist. Whereas the etch plasma damage to the via-sidewall is primarily confined to the surface, a PR plasma strip may induce damage that extends far into the bulk of the ILD and is a function of the overall porosity, pore size and pore interconnectivity.

Following patterning of the via-structure, the line level has to be lithographically defined. In order to allow for uniform coverage of the photoresist on top of the via-structures, the topography has to be planarized. This leveling of the topography is achieved in the so-called via-fill step employing a low molecular weight organic planarizing layer (OPL) [40–42]. The low molecular weight allows for high solids content formulations with correspondingly low viscosities, providing for the ability to fill narrow spaces and to planarize. This ability to fill narrow spaces may present a drawback for porous ILDs with larger and interconnected pores. Here, the OPL may actually penetrate into the ILD (Figure 1.3 (d)). Furthermore, since OPL polymers are generally polydisperse, the penetration problem is exacerbated by the lowest molecular weight species from the low end of the molecular weight distribution. The issue of OPL penetration is just starting to emerge as *k* values are driven to ever lower values. Hopefully, solutions to this problem can be found in a new generation of OPL candidates with properly chosen molecular weight characteristics, by designing high-porosity materials with small, noninterconnected pores or by pore sealing approaches.

Once the structure has been planarized using an OPL, deposition of a low-temperature plasma-deposited oxide layer follows, which allows rework of the PR deposited in the next step. PR deposition is then followed by lithographic patterning and etching the line levels into the ILD, leaving a small plug of OPL at the bottom of the via-structure. This protects the bottom capping layer and is subsequently removed during the PR strip.

However, since the line does not extend all the way to the bottom of the ILD layer, line bottom roughness (LBR) due to a nonhomogeneous etch front may be observed (see Figure 1.3 (e)) [43].

The LBR can then be further exacerbated along with additional sidewall damage to both the line and via, as shown in Figure 1.3 (c), (e) and (f), from the PR strip/OPL clean-out step, which typically requires oxidative plasma conditions. LBR appears to be strongly affected by ILD porosity and pore interconnectivity, even leading to pitting of the line bottom at high porosity levels.

Once the line/via-structures have been defined, another etch step is required to open the capping layer, allowing for the eventual connection of the new line/via level to the underlying metal level. The nature of the cap material dictates plasma etch conditions of this cap-open step, which are even more aggressive, thus exposing the line bottom to further damage (see Figure 1.3 (g)) [44]. In order to mitigate the plasma damage and to remove any plasma residues from the various exposed surfaces, wet-clean processes using dilute HF (DHF) are often employed [45–47]. This treatment ensures good contact between the via and the underlying copper metal as well as removing hydrophilic sidewall damage resulting from the various process plasmas. In the case where sidewall damage was very severe, the wet-clean process can potentially remove so much material as to significantly change the critical dimensions of the line/via-structures.

After the line/via-structures have been defined and the via bottom has been opened to the underlying metal layer, metallization is performed. The metallization portion of the process consists of two steps:

1. barrier layer deposition and
2. Cu plating.

The barrier is generally a bilayer consisting of a metal nitride and a barrier metal to protect the ILD from Cu migration/penetration and typical examples are TaN/Ta and TiN/Ti. The function of the metal nitride is to provide excellent adhesion to the ILD, whereas the barrier metal provides an optimum interface to the Cu. For maximum effectiveness, this barrier layer needs to be continuous and without defects and pinholes. For highly porous ILDs, this requires the use of relatively thick barrier layers to seal off the pores, preventing Cu intrusion into the ILD, as shown in Figure 1.3 (h) [48, 49]. However, as line and via dimensions shrink in accordance with future technology nodes, thinner barrier layers are needed to maintain or improve electrical performance. This requirement presents a major challenge for highly porous materials and may, in fact, limit the extendibility of porous ILDs to dielectric constants >2.0. Next, copper is deposited into the patterned dual-damascene structure and the Cu overburden including the bilayer hardmask is polished back to the ILD using chemical mechanical polishing (CMP). Here, high mechanical forces and the chemical nature of the CMP slurry may adversely affect the stack in the form of adhesive failure at the various interfaces, cohesive failure of the ILD [50–52] and adversely impacting the electrical properties [53] (see Figure 1.3 (i)). Proper selection of the CMP slurries in addition to low down-force CMP processes can significantly mitigate these problems.

Finally, the last step in the dual-damascene process involves the deposition of a capping layer to protect the oxidatively sensitive Cu metallurgy, so that the entire process sequence can be repeated over and over again.

1.2.2 Mechanical Properties

For traditional PECVD and spin-on materials, the mechanical strength of ultra-low-*k* films decreases as the dielectric constant is reduced. Consequently, their stiffness and resistance to cohesive or adhesive fracture is strongly affected. In addition, the number of ULK levels usually increases from one technology node to the next to minimize the BEOL RC_{delay}. On the other hand, the stiffness of controlled-collapsed-chip-connection (C4) solders has increased with the switch to lead-free materials and ceramic carriers have been replaced by organic substrates (with a higher coefficient of thermal expansion (CTE) and lower Young's modulus). Altogether, more thermomechanical stress is applied to the BEOL levels whereas the overall fracture resistance of the structure has been reduced. This conflicting trend in chip–package materials is summarized in Table 1.1 [54, 55].

It is very interesting to note in Table 1.1 that the preferred evolution of BEOL and packaging characteristics is the mirror image to what is currently developed in the semiconductor industry. It is then not surprising that critical reliability issues have been encountered during chip–package interaction (CPI) [56, 57]. Indeed, the thermal deformation of the packaging structure is directly coupled into the BEOL interconnects, creating large stresses at the ultra-low-*k* levels that can induce materials fracture and/or delamination [58]. A good example of such a failure is presented in Figure 1.4 and is known as the 'white bump' issue. These 'white bumps' are observed by acoustic wave spectroscopy (Figure 1.4(a)) after the chip join reflow processing once the flip-chip ball interconnects have solidified [58]. The presence of these 'white spots' indicates that fracture (adhesive or cohesive) occurred

Table 1.1 *Conflicting trend in chip–package material*

	BEOL		Packaging		Substrate flexibility
	ULK Young's modulus	ULK cohesive strength	ULK levels	C4 stiffness	
Preferred	↑	↑	↓	↓	↓
Reality	↓	↓	↑	↑	↑

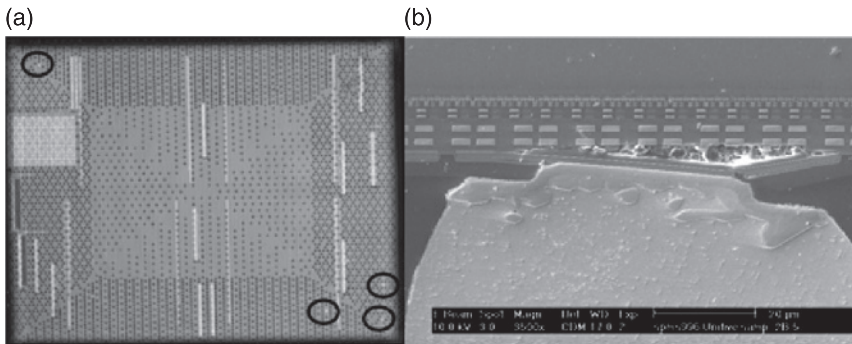

Figure 1.4 *(a) Acoustic wave spectroscopy image of white bumps. (b) Cross-section of a white bump*

underneath the solder ball, usually at the ULK levels (Figure 1.4(b)). It has also been observed that these 'white bumps' were generated during the thermal testing of packaged dies (microprocessors must pass a thousand cycles from sub 0 °C to greater than 100 °C).

Since this failure mechanism is only observed after packaging and thermal testing the cycle of trial and error can be long and expensive. At the same time, new materials are also introduced in the BEOL and at the packaging level for each technology node. Consequently, the identification of the main factors involved with CPI failures in Cu/low-*k* interconnects is a daunting task. In that regard, finite element based modeling coupled with fracture mechanics has been of great help in pinpointing these determining factors. Early on, it was found using three-dimensional (3D) finite element analysis based on a multilevel submodeling approach that for a stand-alone chip, the energy release rate (ERR) induced during processing was lower than the critical ERR for interfacial delamination obtained from a four-point bend test [59]. After the die is assembled in a flip-chip package, a significant increase of this ERR was obtained for the interconnect structure interfaces parallel to the die surface. In a two-metal layer interconnect structure, the ERR was shown to increase rapidly when the modulus of the ILD is lower than 10 GPa [60]. In a more complex structure, the interface exposed to the highest ERR varies as a function of the materials (TEOS, low-*k* and ULK) used at each interconnect level [60]. For a full interconnect structure based on the 65 nm technology node, the ERR increased with increasing crack length. A similar observation has been made by different authors, confirming that the crack feeds from the energy supplied by the package until a steady state is reached [61].

The packaging challenges for ultra-low dielectric materials may be summarized as follows [62]:

– die separation process = dicing,
– underfill selection for ULK and bump protection,
– lead-free bump, with higher stress on ULK levels and
– fine-pitch bump application.

If not addressed, the mechanical issues for BEOL interconnect and packaging will lead to more and more difficulties in successfully passing reliability testing when moving from one technology node to the next. Traditionally seen as two independent sectors, BEOL and packaging must now face the same challenge and a common effort of these two communities is required, i.e. wafer design/manufacturing needs to integrate packaging into the total solution. We believe that opportunities will emerge from a combination of new gentler integration processes, toughening post-treatments, development of stiffer and more crack-resistant advanced ULK materials, implementation of more compliant packaging materials and novel BEOL and packaging designs [55, 62].

1.3 Processing Approaches to Existing Integration Issues

Considering all the integration challenges described in the previous section, the semiconductor industry was faced with two choices:

– develop new processing/engineering solutions or
– design advanced dielectric materials.

Obviously, for a conservative industry, the former represented the more prudent and readily implementable approach. Therefore, much of the initial attention was focused on this area.

In general, these processing/engineering solutions can be divided into three distinct categories:

1. Post-deposition treatments to enhance the physical properties of highly porous dielectric materials.
2. Prevention or repair of plasma-induced processing damage.
3. Use of multilayer structures comprised of an organic dielectric and an organosilicate.

1.3.1 Post-deposition Treatments

The deposition of organosilicate-based dielectric materials, as practiced in the semiconductor industry, typically involves a thermally activated process either during or immediately following the deposition step. The thermal portion of this process step is dictated by the need to decompose the thermally labile pore generator (porogen) and to ensure optimum network formation. Both requirements are favored by high curing temperatures, typically in excess of 400 °C. Network formation and hence mechanical properties greatly benefit from high curing temperatures, as shown by laser spike annealing studies of spin-on organosilicate films [63]. Keeping in mind that for microelectronic applications, temperatures of 400–425 °C are considered an upper limit and curing times are only on the order of several minutes, dielectric films are most likely to be undercured and network formation is not optimized. Although this may not have presented a problem for dense dielectric materials, it is significantly more critical for highly porous coatings with commensurately lower modulus and hardness values. In order to address these weaknesses, thermally assisted e-beam and ultraviolet (UV) curing processes were auditioned. The goal was to facilitate the complete porogen removal at temperatures ≤400 °C and to boost mechanical properties as a result of the known hardening effect of these treatments [64–69].

Of the two radiation processes, e-beam treatments were investigated first, but when it was found that UV irradiation was nearly as effective in promoting complete porogen decomposition and mechanical properties enhancement, the former was dropped due to perceived detrimental effects to the front-end devices [70]. Overall, both processes are similar in that optimum results are generally obtained at 400 °C with exposures typically ranging from 3 to 10 minutes [71–73], the primary difference being that e-beam exposure appears to be more directional as compared to broadband UV exposure [67]. Furthermore, both treatments are equally effective in promoting porogen decomposition at 400 °C [67, 68]. For example, XPS data obtained for porogen containing PECVD organosilicate films as a function of UV exposure at 400 °C indicates a rapid decrease in the C/Si ratio during the first 10 minutes of UV exposure, followed by a significantly lower rate of carbon loss [74]. The initial rapid carbon loss was attributed to porogen decomposition, while the slower change in C concentration was associated with other carbon depleting changes, *vide infra*. However, completeness of the porogen decomposition is not always readily assessable and the presence of porogen residues can persist even after an extended thermally assisted UV cure [75].

For the remainder of this discussion the main focus will be on UV post-deposition treatment, unless there is a specific call for e-beam examples. In addition, primary consideration will be given to broadband UV radiation ($\lambda = 200$–400 nm) over monochromatic UV radiation ($\lambda < 200$ nm) due to the fact that the former is better suited for porogen removal and mechanical enhancement [76], less damaging to the dielectric material [77], less prone to standing wave effects [78, 79] and the preferred spectral range of presently used manufacturing tools.

Spectroscopic examination by Fourier transform infrared (FTIR) and ^{29}Si-NMR of organosilicates exposed to thermally assisted radiation treatments provides a relatively consistent picture of the structural changes taking place. The main observed structural change is an increase in the network connectivity via additional condensation reactions. This is most clearly demonstrated when comparing the ^{29}Si-NMR spectra of pristine and UV-treated films, which exhibit an increase in *Q* (Si bonded to four oxygens) and *T* (Si bonded to three oxygens) moieties of 7 % and 4 %, respectively, after UV exposure [72]. The increase in *T* and *Q* occurs at the expense of *D* (Si bonded to two oxygens) and the complete disappearance of *M* (Si bonded to one oxygen) structural units. In addition, there is a decrease in *T* and *D* structural units with pendant silanol groups. The overall effect is an increase in the degree of condensation, i.e. the degree of cross-linking or network connectivity. Similar and consistent observations were reported by other groups [67, 80]. Complimentary FTIR studies provided additional information and subtleties not apparent from the nuclear magnetic resonance (NMR) experiments. Thus, radiation treated films exhibit a definite change in the Si–O–Si bond arrangement reflected in the 1200–1000 cm^{-1} spectral range. There is a definite decrease in the 1140 cm^{-1} absorption (assigned to the Si–O–Si cage network structure or large bond angle structure) and a concomitant increase in the absorption at 1040 cm^{-1} (assigned to the Si–O–Si small bond angle structure and suboxide). It is not certain whether this structural rearrangement in the Si–O–Si backbone structure results in an overall increase in network connectivity, but the more stable (140–144 ° bond angle) bonding configuration is expected to increase the overall rigidity of the network and hence Young's modulus. Along with these major structural changes, there are smaller observed differences, such as small decreases in the Si–CH_3 absorptions at 2975 cm^{-1}, 2910 cm^{-1} and 1275 cm^{-1} and the appearance of Si–H absorptions at 2240 and 2180 cm^{-1}. Based on these observations it is possible to postulate a series of potential reactions that would account for the spectroscopic data as shown in Figure 1.5. Of these reactions, those represented by pathways (a) to (c) are consistent with experimental observations, with pathway (a) being the most dominant and the other two playing a lesser role. Pathways (d) and (e) lead to carbon-bridged Si-network structures. Although reactions (d) and (e) cannot be totally ruled out, there is a strong possibility that these may arise from residual porogen fragments left in the organosilicate matrix [67, 81]. Finally, reaction pathway (f) has been proposed based on the observed production of Si–H bonds in both UV and e-beam treated organosilicate samples [67, 68, 81]. This reaction is more predominant in e-beam treated samples. However, the relative amount of Si–H formation during UV or e-beam exposure is hard to quantify since this moiety is rather reactive and could be readily consumed by reaction pathway (c). Nevertheless, the presence of residual Si–H bonds is not desirable and presents another reason why broadband UV exposure, with little or no Si–H formation, is preferred.

With an understanding of the underlying structural changes accompanying UV or e-beam exposure of organosilicates, it is now possible to elucidate the observed changes in

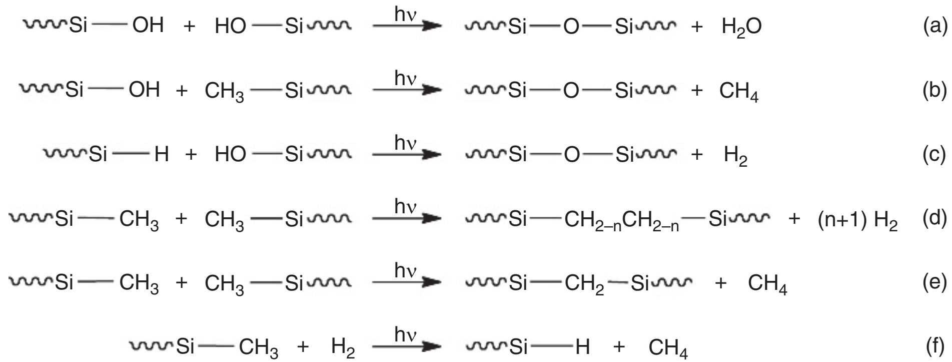

Figure 1.5 *Possible structural modifications iinduced by e-beam or UV exposure of organosilicate materials*

mechanical properties. In general, broadband UV exposure at 400 °C and exposure times on the order of less than 10 minutes lead to a dramatic improvement in Young's modulus (40–50 % increase) while typically slightly lowering the dielectric constant [68, 71, 72, 79]. However, treatment of multistack structures appears less effective and dictates the treatment of individual layers for optimum results [71]. As shown in Figure 1.5, reactions (a) to (c) increase network connectivity, increasing E while consuming pendant Si–OH groups, which leads to a decrease in k due to lower polarizability of the matrix and less propensity to absorb atmospheric moisture. Futhermore, the organosilicate bond rearrangement of UV exposed samples contributes to additional stiffening of the matrix and a concomitant increase in E. This contribution, although not obvious, was elegantly demonstrated by comparing a PECVD organosilicate resin, resin A, with a thermally cured spin-on organosilicate resin, resin B [82]. Resin A, prior to UV exposure, was characterized by low network connectivity, i.e. the presence of significant Si–OH groups. UV cure of this resin exhibited a significant increase in Q groups of the Si-NMR spectrum and little or no Si–O–Si bond rearrangement as reflected in the FTIR spectrum. In contrast, resin B showed high network connectivity, as reflected by the lack of M and D groups in the Si-NMR spectrum. This was not completely unexpected since this resin had been subjected to an initial thermal cure. UV exposure of resin B yielded little or no increase in Q groups, but a noticeable decrease in the large-angle Si–O–Si structure was evident from the FTIR spectrum. Given that both materials exhibited a similar improvement in Young's modulus, the connection between mechanical enhancement by an increase in network connectivity and/or Si–O–Si bond rearrangement could be made. Furthermore, a decrease of Poisson's ratio as a function of UV cure for organosilicate films suggests that increases in the shear modulus dominate over increases in the bulk and/or compressive modulus [82].

Besides the improvement in the stiffness of UV-treated organosilicate materials, the impact of UV curing on the fracture energy was also studied. In this connection, it was shown that while adhesive fracture energies at the top interface can improve by as much as 200 %, cohesive fracture energies and bottom adhesive fracture energies improve at best by 20 %. This suggests a depth dependence of the UV cure. Indeed, studies using monochromatic UV radiation, where the depth dependence is significantly more severe, indicate UV light interference, which forms a standing wave during the curing process [78, 79]. While

underlying layers of transparent SiN can mitigate this effect and increase the adhesive fracture energy at the bottom interface, UV absorbing spacers such as SiCN negated the beneficial effects of UV irradiation at both interfaces [83]. The lack or presence of contributions by thermally assisted UV treatment on the cohesive strength may in fact be due to differences in the nature of the dielectric material and/or the degree of initial network connectivity. Thus, comparison of two distinctly different organosilicates, subjected to identical UV treatment, indicated that cohesive strength is primarily affected by the Si–O–Si large-angle bond rearrangement [82]. Furthermore, there seems to be no significant change in the threshold or subcritical crack growth velocity although the underlying reasons are still being debated [73, 81, 84].

To summarize, thermally assisted broadband UV treatment of organosilicates is very effective in facilitating porogen removal, minimizing the thermal budget and increasing Young's modulus. This enhancement of the mechanical properties is a prerequisite in being able to go to higher porosities (lower k values) and in turn extending the technology to future device generations. It should be noted that along with the beneficial effects of such post-deposition treatments on the dielectric insulator there might also be less understood implications with respect to underlying structures, such as capping layers, etc. Obviously, more studies are necessary in this area.

1.3.2 Prevention or Repair of Plasma-Induced Processing Damage

As the dielectric constant of the ILD is pushed to lower values, larger and highly interconnected pores are created, raising the following concerns:

– access of reactive plasmas deeper into the ILD,
– OPL penetration into the ILD and
– noncontinuous barrier layer coverage at the sidewall leading to metal intrusion.

Of course, the majority of these problems could be addressed by generating the porosity after the DD structure build is completed. This has been proposed in a 'solids first' or 'porosity last' approach [85–89]. In these schemes the porosity is created either after etch (PEBO) or after Cu CMP (PCBO), the latter requiring the use of a permeable cap. Furthermore, the PCBO approach is more desirable based on the fact that it protects from plasma damage, minimizes liner discontinuities and eliminates metal intrusion. Either way, considerable improvements in reliability and downscaling of the metal barrier could be realized. However, these advantages are in the least partially negated by large ILD shrinkage (~ 10 %) upon porogen burn-out. As a result, this approach has not been pursued any further.

Another alternative is to seal the surface of the porous interfaces. This approach addresses barrier metal coverage and prevention of metal intrusion, but has no effect in mitigating plasma damage. Nevertheless, two potential pathways have been explored. The first pathway interposes a thin, continuous layer between the porous ILD and the barrier metal [90, 91]. This material could be deposited by various means and both organic and inorganic candidates have been proposed [25, 48, 49, 92–95]. Furthermore, since this material contributes to the overall dielectric constant, candidates with relatively low k values are preferred.

Potential drawbacks to this approach present themselves in the introduction of new material interfaces and the need to remove the additional material at the via bottom. Thus,

the former could give rise to interfacial adhesion issues, while the latter could adversely affect the cap-open step to establish metal contact.

The second pathway to pore sealing is by plasma modification. Proper selection of a suitable plasma may densify the outermost surface of the via and line sidewalls, enabling deposition of thin, continuous barrier layers [96–101]. As it turns out, this approach is feasible for microporous dielectric materials, i.e. small pores with little or no interconnectivity, but fails for mesoporous materials. Due to the high interconnectivity of mesoporous materials, plasma modification is not merely restricted to the surface but penetrates deep into the bulk of the material. Here dielectric damage appears to dominate with only limited pore-sealing success.

Whereas these two modifications address the issue of smooth sidewalls for optimum barrier metal deposition, they do not consider the plasma damage to the ILD from etch and strip processes. Although strip (resist removal) damage can be minimized with the use of hardmasks (the lithographic pattern is first transferred to the hardmask, which allows a PR strip without exposing the ILD) [29, 30, 102–105], plasma damage arising from the actual ILD etch cannot be neglected. This damage manifests itself in the form of oxidative degradation of the ILD and as a result produces silica-based oxides and hydroxides at the exposed surfaces. The presence of the latter is particularly detrimental to the dielectric constant due to its propensity to absorb moisture. In addition, the effect of the oxidative ILD damage on the mechanical properties is still uncertain.

Given that plasma damage is hard to prevent, the alternative is to repair this damage. In this respect, two techniques have emerged. The first technique tries to make use of a hydrogen plasma treatment, which converts the damaged layer to a denser layer of Si–H rich material [106–109]. In addition, the porous matrix material may experience rearrangement of the Si bonds to include formation of $Si(CH_3)_3$, $SiOCH_3$ and Si–C bonds, while also suffering from a reduction in the Si–CH_3 bonds [110, 111]. Of course, the extent of plasma damage is dependent on the specific plasma conditions [112].

The second process utilizes reactive silylating agents to convert hydrophilic Si–OH groups into hydrophobic derivatives [113–119]. This reaction is best accomplished with highly reactive chlorosilanes, but the corrosive nature of the by-product HCl and the potential to introduce chloride ions makes them poor candidates. Much more suitable silylating agents are silylamines, such as hexamethyldisilazane and dialkylaminotrimethylsilane, which only generate nonhalogen containing by-products. Here, the difficulty lies in the delivery of these reagents in order to maximize the penetration into the porous dielectric resin. Although solvent mediated treatments have been proposed, only supercritical CO_2 (SCO2) or gas-phase treatments are of practical value [120–122]. Gas-phase silylation is particularly attractive since this restoration process uses a neat reagent at elevated temperatures, greatly amplifying the reactivity of the nonhalogen containing candidates. However, even in the best of situations, the silylation process cannot fully restore the damage ILD to its previous virgin state [113].

1.3.3 Multilayer Structures

Finally, plasma damage can be mitigated by the presence of high carbon content materials. This observation was utilized in hybrid integration approaches, which utilize a two-layer ILD comprised of an organosilicate layer at the via level and an organic polymer

layer at the trench level [8, 123–125]. Although this approach limits plasma damage mainly to the via level (top and sidewall surfaces), it complicates the integration approach. Thus, since most organic polymers, e.g. polyarylenes or poly(arylene ethers), are deposited by spin-on techniques and the majority of organosilicate materials are prepared by PECVD, two distinctly different deposition tool sets would be required. Furthermore, the introduction of new interfaces, as mentioned previously for pore sealing using thin liners, may significantly affect interfacial adhesion. One novel integration approach combines both hybrid integration (useful for minimizing ILD damage at the trench level) and a new concept referred to as 'effective porogen control' (ECB) [126]. The latter is achieved by limiting the amount of porogen decomposition of the porous SiCOH layer, i.e. the via level, to less than 70 %. The remaining porogen effectively increases the carbon content of this layer protecting the via level. The remaining porogen is partially removed during the plasma processing steps (trench level), followed by a thermal cure after a complete DD build.

1.4 Material Advances to Overcome Current Limitations

In the search for improved mechanical properties of highly porous materials, two candidates have emerged over the past few years. The first type, strictly spin-on, is based on the superior mechanical properties of crystalline zeolites. The second type of material relies on maintaining a highly connected network by introducing carbon as a bridging group in between the silicon atoms. Initially developed for spin-on materials, the latter strategy has been also recently adopted by the PECVD community. Carbon-bridged CVD precursors have appeared to replace current materials for the 32 nm technology node and beyond.

1.4.1 Silica Zeolites

Zeolites (derived from the Greek words *zeo* (to boil) and *lithos* (stone)) are microporous crystalline materials that consist of open aluminosilicate frameworks derived from $[SiO_4]^{4-}$ and $[AlO_4]^{5-}$ tetrahedra linked to form cages, channels or cavities of various sizes [127]. The negatively charged frameworks are balanced by positively charged cations of appropriate size located at various positions in the lattice. Because of their well-defined micropores and the presence of acidic sites inside the pores, zeolites have been successfully employed for a diverse range of applications: ion exchange, separations and catalysis (oil refining, petrochemistry, organic synthesis) [128]. While pure-silica zeolites, silicalite-1 (similar to ZSM-5) [129] and silicalite-2 (similar to ZSM-11) [130], were synthesized for the first time at the end of the 1970s, it is not until recently that these materials have received some attention from semiconductor manufacturers as potential low-k dielectrics. Since silicon is tetravalent, pure-silica zeolites (PSZs) do not contain framework charges and consequently no cations, which would be detrimental for electronic applications, are present. Due to their dense crystalline structure, better mechanical properties are expected [131], and since their pore size (<2 nm) is significantly smaller than integrated circuit (IC) features, the problem of electrical breakdown should be mitigated by the absence of any randomly occurring large pores.

The first films made of silica zeolites were obtained following two strategies [132]:

(a) in situ crystallization in a Teflon-lined Parr autoclave (165 °C, 2h) of a solution composed of 0.32 TPAOH/TEOS/165 H_2O and
(b) spin-coating of a silicalite nanocrystals containing solution [132–134].

Independent of the method used to grow silicalite films, a post-synthesis thermal treatment at 450 °C for 2 hours is applied to remove the tetrapropylammonium hydroxide (TPAOH) template.

In the case of in situ crystallized films, thicknesses vary from 200 to 500 nm, and chemical mechanical polishing (CMP) needs to be performed initially to smooth the surface. These films possess excellent mechanical properties with E = 30–40 GPa (nanoindentation) for dielectric constants ranging from 2.7 to 3.1. The effect of water adsorption on the k value of silicalite films was examined by exposing the sample to air at 60 % relative humidity. The k value increases from 2.7 to 3.3 after an exposure time of 30 h (k = 3.5 after several days). This observation is in good agreement with an ellipsometric porosimetry (EP) study using water as an adsorbent, reporting that the in situ crystallized film's hydrophilicity increases with aging [135].

On the other hand, silicalite spin-on films present lower dielectric constants (k = 1.8–2.1) due to the additional porosity gained from internanocrystal packing voids [132]. A uniform interparticle pore size of 17 nm and an interparticle pore volume of 0.40 $cm^3\ g^{-1}$ were measured by N_2 adsorption experiments performed on bulk samples. While beneficial in terms of the dielectric constant, the presence of larger mesopores is not only of concern for practical applications but also affects the adhesive properties of these films, leading to failure during CMP [136]. To address this issue, a brief secondary growth of silicalite nanocrystals can be applied, resulting in the loss of the interstitial porosity, an increase of the dielectric constant to a value of 3.0 and restoration of the adhesive properties observed for the in situ crystallized films. This second silicalite growth can be avoided by using an amorphous silica containing silicalite nanocrystals solution. Here, the mesopore size is reduced from 17 to 2.3–2.6 nm, resulting in a film with better mechanical properties (E = 16–18 GPa by nanoindentation) and a dielectric constant of 2.3 [137]. Positronium annihilation fifetime spectroscopy (PALS) was used in this case to confirm the presence of micropores (0.55 nm) due to the zeolite framework, in addition to open/interconnected mesopores (2.3–2.6 nm) [138]. Unfortunately the film is quite hydrophilic, as shown by an increase in the dielectric constant from 2.3 to 3.9 within 1 h of exposure to ambient air at 50–60 % relative humidity. To render the film hydrophobic, vapor-phase silylation was conducted. After silylation, a dielectric constant of 2.1 was obtained; this value changes slightly over time upon exposure to air. Interestingly, this post-curing treatment step can be eliminated if the silylation is performed during the zeolite synthesis and/or during calcination of the template [139].

In order to achieve a tunable k value in an even lower range on the MFI (zeolite with a two-dimensional 10-ring pore structure and pore size of 5.5Å) low-k material, incorporation of nanosized voids using γ-cyclodextrin as a porogen was explored [140]. By introducing 5–15 wt % of γ-cyclodextrin, controllable interparticle porosity ranging from 2.71 to 3.29 nm was created. The dielectric constant decreases in relation to the amount of porogen used. A value of 1.8 is obtained for a 15 wt % porogen loading, while the mechanical properties for this film remain excellent (E = 14.3 GPa by nanoindentation). Unfortunately, all of the cyclodextrin containing films required heating to 450 °C for 9 h to ensure full decomposition of the porogens (cyclodextrin and TPAOH), making this process unsuitable for integration.

Because all the films above are composed of a mixture of amorphous silica and silicalite nanocrystals, not only the overall ratio of one silica component versus the other (in other words the total level of film crystallinity) [141] but also the nature of the zeolite (MFI or MEL, zeolites with a two-dimensional 10-ring pore structure) [142] influence the dielectric properties of the material. Using a two-stage hydrothermal synthesis method, the yield of nanocrystals for a given particle size can be increased in the solution used for film preparation. A direct effect is observed on the dielectric constant of the films with higher crystallinity, leading to lower *k* values [141, 142]. At the same relative level of crystallinity, changing the nature of the zeolite nanocrystals from MFI to MEL also results in a lower dielectric constant. The authors point out that a lower *k* value is expected because MEL has a lower framework density (FD) than MFI [142]. Since different sizes of nanocrystals are used in this study and the total porous volume of the films is different, it is not clear whether this result can be directly correlated to the nature of the zeolite or if it is governed by other parameters such as the size of the nanocrystals, mesoporous volume and number of residual silanols. Without silylation, and independent of the level of crystallinity, the synthesized films are still highly hydrophilic.

While this strategy initially looks very attractive, it is worth noting that the longer the second crystallization stage (i.e. higher crystallinity), the lower the mechanical properties [143, 144] and the bigger the interstitial voids [143, 145]. The mechanical properties decrease with increasing crystallinity because there is less amorphous silica to ensure the homogeneity of the film and also because the interstitial volume and size increase as well [143]. Regarding the last point, it was clearly shown that for silicalite films the pore size and distribution evolve as a function of the crystallization time [143, 145]. For crystallization times less than 3–4 days, pores at 0.55 nm (from silicalite) and at 2–5 nm are detected. At longer crystallization times, additional pores in the range of tens of nanometers are formed [143, 145]. Furthermore, it has been demonstrated that an increase of crystallinity is accompanied by a growth of the nanocrystal size and a reduction in the relative amount of amorphous silica [146]. It is most likely that these two parameters have a direct effect on the size of the voids. In that regard, Liu *et al.* have developed an 'evaporation-assisted two-stage synthesis that apparently limits the formation of 40–80 nm zeolite nanoparticles in solution leading to low-*k* films with improved properties' [147]. They have reported that small MEL nanocrystals (e.g. 14 nm) could be obtained in a 63 % yield using this strategy. Unfortunately, spin-coating of the above formulation leads to low-*k* films containing pores as wide as 50 nm, as evidenced by a comparative study conducted by a different group [148].

Remarkably, it was recently discovered that crystallization can also occur during the annealing of the spin-on films in a new process called 'on-wafer crystallization' [149]. The formation of big particles in solution is prevented by the absence of any hydrothermal treatment. After anneal and silylation, the film has a dielectric constant of 1.8, a Young's modulus of 16.8 GPa and an average pore size diameter centered around 6 nm. While smaller, the pores are still too big to envision a trouble-free integration of these materials.

Another approach to decrease the pore size diameter of PSZ low-*k* films was developed by Eslava *et al.* [150]. They have shown that UV curing (5 min at 425 °C under an inert atmosphere) of silica zeolite as-synthesized films leads to the formation of mesopores in the 2–8 nm range. For comparison, the calcined film only contains much larger pores in the 10–50 nm range. In addition, the UV-assisted curing not only increases the hydrophobicity of the porous zeolite film by condensation of silanols but also through grafting of the

desorbing organic template fragment, an unexpected result. The film has a dielectric constant of 2.16 and a Young's modulus of 10.7 GPa. While the mesopores are again too big for application as a low-*k* dielectric material, UV curing appears as a novel path to the design of PSZ films with the desired mechanical, electrical and pore size distribution properties. In a more recent publication, post-deposition UV curing was combined with two silylation steps using 1,3,5,7-tetramethylcyclotetrasiloxane (TMCTS) [151]. The film modulus improved from 4.2 to 10 GPa after the complete treatment, for a dielectric constant $k = 2.18$. It is worth noting that no pore size distribution was reported in this paper [151].

A different strategy to address the water adsorption in PSZ films is to synthesize organic-functionalized PSZ MFI films (OF PSZ) [152]. Incorporation of Si–Me groups in the zeolite framework was achieved through addition of $MeSi(OMe)_3$ to the synthesis solution of MFI nanoparticles. Upon exposure to ambient air for 1 h, the dielectric constant of the OF PSZ film increased from 2.25 to 2.74 (20 %), compared to a 70 % increase for the nonfunctionalized film (10 % after silylation). Other organic groups, different from Si–Me, 3,3,3-trifluoropropyltrimethoxysilane (C6) or 1*H*,1*H*,2*H*,2*H*-perfluorooctyltriethoxysilane (C14), have also been used to functionalize PSZ MFI and PSZ MEL [153]. In this case, the quantity of water adsorbed, while reduced, is still significant. The amount of organic groups incorporated, initially low to preserve the crystalline structure, is reduced even further after calcination due to partial decomposition, possibly explaining why higher hydrophobicity is not achieved. Interestingly, OF PSZ films have also been mixed with an organosilicate (50 % MTES/50 % TEOS) containing F127, a triblock porogen of the Pluronics® family [154]. No post-calcination silylation is necessary when the amount of OF PSZ is kept below 20 %. However, the Young's modulus value and the pore size distribution reported in this paper [154] are questionable.

In the case of OF PSZ films, it has been clearly shown that the introduction of Si–Me groups significantly increases the hydrophobicity of the film but also affects its level of crystallinity [155]. The authors mimicked the synthesis of silicalite using the following solution composition: $0.5MTMS/0.5TEOS/5H_2O/0.2TPAOH$ [155]. The film is amorphous and has been named ZLK (zeolite-inspired low-*k*). This film is microporous (no pores bigger than 2 nm) and has a dielectric constant of 2.2 that only increases by 0.5 % upon exposure to ambient air. The Young's modulus was measured by nanoindentation and is in the 6–7 GPa range.

As of today, the major drawbacks associated with the preparation of zeolite films, such as, big nanoparticles, hydrophilicity and the presence of big mesopores, have not been fully solved. For these reasons the use of silicalite films as future low-*k* materials in semiconductor manufacturing does not seem realistic at this time. An exception are ZLK films, which exhibit the expected properties to warrant some integration work. Nevertheless, their properties are similar to those reported for oxycarbosilane materials [1], which are prepared by nonhydrothermal synthesis and are easily scalable.

1.4.2 Hybrid Organic–Inorganic: Oxycarbosilanes

The observation that incorporation of organic moieties into sol-gel glasses can reduce their brittleness [156–160] has drawn the attention of the semiconductor industry. However, in order to be viable candidates for application in the BEOL, the silicon precursors to these

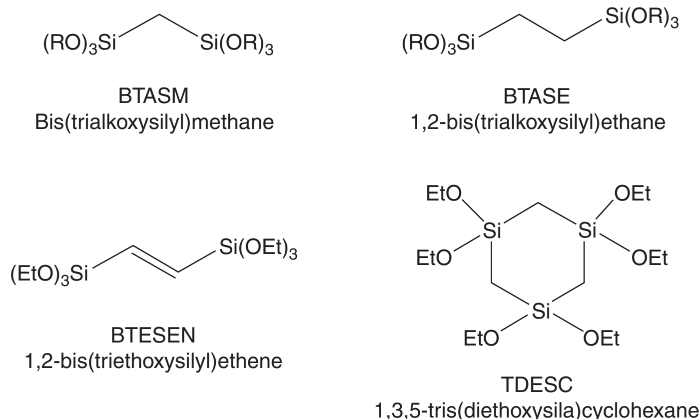

Figure 1.6 *Carbon-bridged alkoxysilane precursors used in the preparation of spin-on porous low-*k *films (R = OMe, OEt)*

hybrid materials should be low cost, commercially available or readily prepared on a large scale. For these reasons, the choice has been limited to simple alkoxysilane molecules containing a carbon bridge between the silicon atoms (Figure 1.6). These hybrid organic–inorganic materials are known in the literature under different names: bridged polysilsesquioxanes [161, 162], oxycarbosilanes [1, 7, 163–165] and carbosiloxanes [166]. Similarly to traditional organosilicates, they are stable up to 425–450 °C in an inert atmosphere and incorporation of a certain level of porosity is necessary to achieve *k* values below 2.4. Although the physical properties of the porous films are in part dependent on the type of porogen used, the chemical nature of the hybrid network is more important [1]. In this regard, the mechanical properties vary significantly for materials prepared in the presence of a coprecursor (e.g. MTMS) rather than from the single monomer.

Different authors have studied the properties of porous thin films prepared from MTMS/BTASM [167] or MTMS/BTASE [168–171] mixtures with a porogen. Unfortunately, full characterization, i.e. dielectric constant, Young's modulus and pore size distribution, was not reported for a given composition. Nevertheless, it was observed that at a dielectric constant of ~2.3, the Young's modulus doubles when the MTMS/BTASE ratio is increased from 100:10 to 100:90 [169]. This result is in good agreement with a study on neat films showing the significant impact on the Young's modulus of adding 10 to 100 mol % of BTASE to MTMS [172]. Still, the addition of porosity to MTMS/BTASE copolymers leads to an important decrease of the mechanical properties, even at low porogen loadings. This is due to the power law decay of the modulus as a function of porosity, typically observed for organosilicates [1].

BTASM, BTASE, BTESEN and TDESC have also been mixed with TEOS (or TMOS) and a surfactant to produce periodic mesoporous organosilicate low-*k* films [13, 173–175]. Materials with a dielectric constant in the 2.0 range were easily accessible using the above strategy. However, the question remains whether a controlled and reproducible level of pore organization over a very large surface is possible in a manufacturing environment. Indeed, differences in pore organization across the wafer would result in material properties variability and lack of etch uniformity. As of today, no integration data have been reported for these materials and therefore their potential is still difficult to assess.

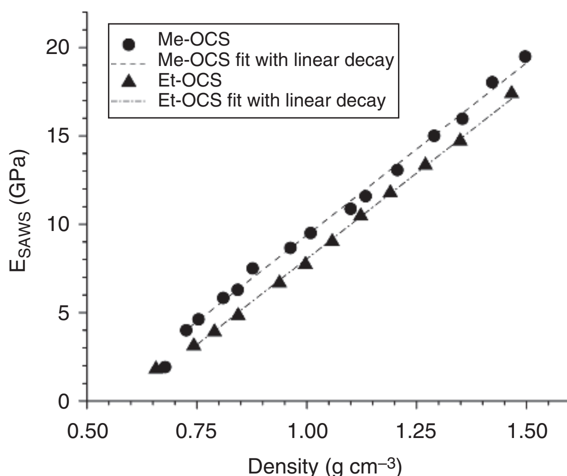

Figure 1.7 *Young's modulus for Me-OCS and Et-OCS as a function of density*

Our strategy to prepare hybrid organic–inorganic low-*k* films focused on two aspects: (a) compatibility of the sol–gel chemistry and solution deposition with semiconductor requirements and (b) use of oxycarbosilane precursors (BTASM or BTASE) in their neat form. Compared to previous studies, we have developed a process that is compatible with current integration requirements, i.e. the surfactant has to be nonionic and thermally decomposed (extraction by solvent washing was avoided), high-quality films without defects can be spin-coated on 8 in and 12 in wafers (low boiling alcohols cannot be used as a solvent), halogenated acids like HCl need to be replaced by HNO_3 to prevent chloride ion contamination and, finally, sol solutions should be stable for at least one month at room temperature. Regarding the sol–gel chemistry, we have demonstrated that hydrolysis conditions for oxycarbosilane precursors need to be precisely controlled in order to obtain high-quality films with the targeted electrical and mechanical properties. Under acidic conditions, a stoichiometric amount of water or higher is preferred to favor the formation of higher molecular weight polymers and consequently eliminate volatilization of low molecular weight oligomers and cyclics during the baking stage. Furthermore, the stability of 30 wt % oxycarbosilane solutions in 1-methoxy-2-propanol containing a poly(alkylene oxide)-based porogen, water and a catalytic acid was studied over time until the onset of gel formation. At room temperature the prepared formulations were stable for at least one month before a gel is formed. Under optimized conditions, we also found that the poly(alkylene oxide) porogens used needed to contain an ethylene oxide chain of at least 10 units to ensure good compatibility of the polymer with the oxycarbosilane matrix. The mechanical properties for oxycarbosilane films of varying porosity generated using either Pluronic 123® ($-(CH_2-CH_2-O)_{20}-(CH_2-CH-(CH_3)-CH_2)_{70}-(CH_2-CH_2-O)_{20}-$) or Brij 35® ($C_{12}H_{25}(O-CH_2-CH_2)_{23}OH$) were also investigated and are presented in Figure 1.7. Me-OCS and Et-OCS are used here to designate the thermally cured films obtained from BTASM and BTASE, respectively. The Young's modulus decreases linearly with decreasing density (i.e. increasing porosity), which is a unique characteristic of coadditive-free oxycarbosilanes [164, 165]. This result contrasts with SSQ–porogen mixtures where the decay in

modulus is exponential. At a dielectric constant of 2.0, the Young's modulus values by SAWS are ~ 5 and ~ 6 GPa for Et-OCS and Me-OCS, respectively.

The modulus values obtained for thermally cured oxycarbosilane films are by far the largest of any we have observed for porous films generated using the sacrificial porogen route. Similarly, the fracture energies of the oxycarbosilane films are also considerably higher than their CDO and MSSQ counterparts. At a dielectric constant of 2.0, *G* (cohesive) is 2.8 J m^{-2} as compared to 1.5 and 1.3 J m^{-2} for both CDO and MSSQ [164]. Interestingly, recent computational modeling has established fundamental scaling laws for the elastic and fracture properties of hybrid glasses [176]. They have found that for ethane-bridged glasses, the bulk modulus scales as $(p - 0.6)^{1.92}$ and the fracture energy scales as $(p - 0.55)$, with p being the network connectivity. In other words, while Si-Me groups provide significant benefits such as plasma resistance and hydrophobicity, they are detrimental to the mechanical properties because they lower the overall connectivity of the network.

Another strategy to prepare porous carbon-bridging containing materials was recently developed by Rathore *et al.* [166]. Their approach is based on the sol–gel processing of hyperbranched polycarbosiloxanes (HBPCSO). These polymers contain different silicon microenvironments corresponding to $[O_{4-x}Si(CH_2)_x]$, with $x = 1$–4. This constitutes a major difference from Me-OCS where the nominal structure is only composed of $[O_3SiCH_2]$ units. Films with dielectric constants ranging from 3.0 to ~ 1.8 were obtained using Pluronic 123® as a porogen. Over this entire range, Young's moduli obtained for HBPCSO films are largely superior to the MSSQ samples (prepared under similar conditions), but slightly inferior to Me-OCS samples. This observation confirms that silicates containing carbon-bridging groups belong to a different class of materials when considering the mechanical properties of porous low-*k* dielectrics.

Finally, PECVD films prepared from carbon-bridged precursors have also recently emerged to replace current materials at the 32 nm technology node and below [177, 178]. While the generic formula is still proprietary, it is believed that these precursors are based on a methane-bridged (MB) structure. They are typically used in combination with DEMS (diethoxymethylsilane) and BCHD (bicyclohexadiene) to prepare porous films using UV curing and which exhibit *k* values ranging from 2.2 – 2.4 [177, 178]. Interestingly, films prepared from the MB precursor had slightly lower mechanical properties but their porosity was significantly modified. Indeed, at the same dielectric constant, the proportion of ultramicropores (< 10 Å) versus supermicropores (10–20 Å) increases for MB-containing films. These films present a higher resistance to the plasma-induced damage observed during nanofabrication [179]. Knowing that the MB-containing films also possess a higher carbon content, we believed that their superior resistance to plasma-induced damage is the combination of this characteristic and their remarkable porous structure.

1.5 Conclusion

It is definitely an interesting time in the field of low-*k* materials as materials chemistry and process engineering need to come together to facilitate the successful implementation of $k < 2.4$ dielectrics in future technology nodes. Obviously, similar progress is also required for other BEOL materials such as dielectric caps, hardmasks, liners, metallurgy, etc.

The main challenges for ultra-low-k materials are associated with their usually poor mechanical properties and their highly interconnected porous network. The introduction of UV curing in manufacturing has permitted the first generation of $k = 2.4$ PECVD materials to achieve sufficient mechanical properties to be integrated. Beyond this dielectric constant, it is anticipated that new PECVD precursors will have to be implemented in order to satisfy the BEOL mechanical requirements. In that regard, spin-on silicalites, ZLK and oxycarbosilanes offer a significant advantage as their mechanical properties are equivalent or superior to manufactured PECVD $k = 2.4$ materials, at a $k < 2.2$. Among them, oxycarbosilane materials seem to be the most advanced in terms of development. Nevertheless, successful integration at the most aggressive ground rules needs to be demonstrated for these spin-on candidates to attract the full attention of the semiconductor industry. Electrical and mechanical reliability of these structures will be under scrutiny as the effect of plasma-induced damage and pre-clean treatments will become worse with increasing porosity. Toward this goal, it is incumbent that gentler plasma processes and process damage repair need to play a significant role. In the future, the solution might also arise from the combination of these new materials with new and innovative integration schemes [180].

References

[1] Volksen, W., Miller, R.D. and Dubois, G. (2010) Low dielectric constant materials. *Chem. Rev.*, **110**, 56–110.

[2] Goto, K., Akiike, T., Konno, K., Shiba, T., Patz, M., Takahashi, M., Inoue, Y. and Matsubara, M. (2002) Thermally stable polyarylenes with low dielectric constant: direction towards the lowest limit of dielectrics. *J. Photopolym. Sci. Technol.*, **15**, 223–229.

[3] Maier, G. (2001) Low dielectric constant polymers for microelectronics. *Prog. Polym. Sci.*, **26**, 3–65.

[4] Miwa, T. (2001) Polyimides in microelectronics applications. *J. Photopolym. Sci. Technol.*, **14**, 29–32.

[5] Treichel, H., Ruhl, G., Ansmann, P., Wurl, R., Muller, C. and Dietlmeier, M. (1998) Low dielectric constant materials for interlayer dielectric. *Microelectron. Engng*, **40**, 1–19.

[6] Treichel, H., Withers, B., Ruhl, G., Ansmann, P., Wurl, R., Muller, C., Dietlmeier, M. and Maier, G. (1999) Low dielectric constant materials for interlayer dielectrics, in *Handbook of Low and High Dielectric Constant Materials and Their Applications* (ed. Nalwa, H.S.), vol. 1, Academic Press, San Diego, California, pp. 1–71.

[7] Dubois, G., Volksen, W. and Miller, R.D. (2007) Spin-on dielectric materials, in *Dielectric Films for Advanced Microelectronics* (eds Baklanov, M., Maex, K. and Green, M.), John Wiley & Sons, Inc., New York.

[8] Nakamura, T. and Nakashima, A. (2004) Robust multilevel interconnects with a nano-clustering porous low-k ($k < 2.3$). Proceedings of the 7th IEEE International Interconnect Technology Conference, Burlingame, California, pp. 175–177.

[9] Homma, T. (1998) Low dielectric constant materials and methods for interlayer dielectric films in ultralarge-scale integrated circuit multilevel interconnections. *Mater. Sci. Engng, R*, **R23**, 243–285.

[10] Kirk-Othmer (1992) *Kirk-Othmer Encyclopedia of Chemical Technology*, 3rd edn, vol. 20, John Wiley & Sons, Inc., New York, pp. 748–825.

[11] Grill, A. (2007) Low and ultralow dielectric constant films prepared by plasma-enhanced chemical vapor deposition, in *Dielectric Films for Advanced Microelectronics* (eds Baklanov, M., Maex, K. and Green, M.), John Wiley & Sons, Inc., New York.

[12] Grill, A. (2009) Porous pSICOH ultralow-k dielectrics for chip interconnects prepared by PECVD. *Annu. Rev. Mater. Sci.*, **39**, 49–69.

[13] Hatton, B.D., Landskron, K., Hunks, W.J., Bennett, M.R., Shukaris, D., Perovic, D.D. and Ozin, G.A. (2006) Materials chemistry for low-*k* materials. *Mater. Today*, **9**, 22–31.

[14] Hoofman, R.J.O.M., Nguyen, V.H., Arnal, V., Broekaart, M., Gosset, L.G., Besling, W.F.A., Fayolle, M. and Iacopi, F. (2007) Integration of low-*k* dielectric films in damascene processes, in *Dielectric Films for Advanced Microelectronics* (eds Baklanov, M., Maex, K. and Green, M.), John Wiley & Sons, Inc., New York.

[15] Morgen, M., Ryan, E.T., Zhao, J.-H., Hu, C., Cho, T. and Ho, P.S. (2000) Low dielectric constant materials for ULSI interconnects. *Annu. Rev. Mater. Sci.*, **30**, 645–680.

[16] Baklanov, M.R. (2007) Porosity of low dielectric materials. Ellipsometric porosimetry, in *Dielectric Films for Advanced Microelectronics* (eds Baklanov, M., Maex, K. and Green, M.), John Wiley & Sons, Inc., New York.

[17] Gidley, D.W., Peng, H.-g. and Vallery, R. (2007) Porosity of low dielectric materials. Positron annihilation spectroscopy, in *Dielectric Films for Advanced Microelectronics* (eds Baklanov, M., Maex, K. and Green, M.), John Wiley & Sons, Inc., New York.

[18] Maex, K., Baklanov, M.R., Shamiryan, D., Iacopi, F., Brongersma, S.H. and Yanovitskaya, Z.S. (2003) Low dielectric constant materials for microelectronics. *J. Appl. Phys.*, **93**, 8793–8841.

[19] Soles, C.L., Lee, H.-J., Vogt, B.D., Lin, E.K. and Wu, W.-L. (2007) Porosity of low dielectric materials. Structure characterization of nanoporous interlevel dielectric thin films with X-ray and neutron radiation, in *Dielectric Films for Advanced Microelectronics* (eds Baklanov, M., Maex, K. and Green, M.), John Wiley & Sons, Inc., New York.

[20] Wolf, S. (2002) *Silicon Processing for the VLSI Era*, vol. 4, *Deep-Submicron Process Technology*, Lattice Press, Sunset Beach, California.

[21] Chiang, C.-C. Chen, M.-C., Li, L.-J., Wu, Z.-C., Jang, S.-M. and Liang, M.-S. (2004) Physical and barrier properties of amorphous silicon-oxycarbide deposited by PECVD from octamethylcyclotetrasiloxane. *J. Electrochem. Soc.*, **151**, G612–G617.

[22] Chiang, C.-C., Ko, I.H. and Chen, M.-C. (2003) Leakage and breakdown mechanisms in Cu damascene with a bilayer-structured a-SiCN/a-SiC dielectric barrier. Proceedings of the 6th IEEE International Interconnect Technology Conference, Burlingame, California, pp. 201–203.

[23] Chiang, C.-C., Ko, I.H., Chen, M.-C., Wu, Z.-C., Lu, Y.-C., Jang, S.-M. and Liang, M.-S. (2004) Improvement in leakage current and breakdown field of Cu-comb capacitor using a silicon oxycarbide dielectric barrier. *J. Electrochem. Soc.*, **151**, G606–G611.

[24] Martin, J., Filipiak, S., Stephens, T., Huang, F., Aminpur, M., Mueller, J., Demircan, E., Zhao, L., Werking, J., Goldberg, C., Park, S., Sparks, T. and Esber, C. (2002) Integration of SiCN as a low *k* etch stop and Cu passivation in a high performance Cu/low *k* interconnect. Proceedings of the 5th IEEE International Interconnect Technology Conference, Burlingame, California, pp. 42–44.

[25] Tsui, T.Y., Willecke, R. and McKerrow, A.J. (2003) Effects of silicon carbide composition on dielectric barrier voltage ramp and TDDB reliability performance. Proceedings of the 6th IEEE International Interconnect Technology Conference, Burlingame, California, pp. 45–47.

[26] Guyer, E.P., Patz, M. and Dauskardt, R.H. (2006) Fracture of nanoporous methyl silsesquioxane thin-film glasses. *J. Mater. Res.*, **21**, 882–894.

[27] Ong, M.D., Jousseaume, V., Maitrejean, S. and Dauskardt, R.H. (2006) Fracture properties of porous MSSQ films: impact of porogen loading and burnout. Proceedings of the Materials Research Society Symposium, San Francisco, California, pp. 15–20.

[28] Grill, A., Edelstein, D., Lane, M., Patel, V., Gates, S., Restaino, D. and Molis, S. (2008) Interface engineering for high interfacial strength between SiCOH and porous SiCOH interconnect dielectrics and diffusion caps. *J. Appl. Phys.*, **103**, 054104/054101–054104/054106.

[29] Assous, M., Simon, J., Broussous, L., Bourlot, C., Fayolle, M., Louveau, O., Roman, A., Tabouret, E., Feldis, H., Louis, D. and Torres, J. (2003) Porous dielectric dual damascene patterning issues for 65-nm node: Can architecture bring a solution? Proceedings of the 6th IEEE International Interconnect Technology Conference, Burlingame, California, pp. 97–99.

[30] Hiroi, M., Ohtake, H., Saito, S., Onodera, T., Furutake, N., Harada, Y. and Hayashi, Y. (2001) Dual hard mask process for low-*k* porous organosilica dielectric in copper dual damscene interconnect fabrication. Proceedings of the 4th IEEE International Interconnect Technolnology Conference, Burlingame, California, p. 295.

[31] Kinoshita, K., Tada, M., Usami, T., Hiroi, M., Tonegawa, T., Shiba, K., Onodera, T., Tagami, M., Saitoh, S. and Hayashi, Y. (2000) Process design methodology for via-shape-controlled, copper dual-damascene interconnects in low-*k* organic film. Technical Digest – International Electron Devices Meeting, pp. 257–260.

[32] Fayolle, M., Torres, J., Passemard, G., Fusalba, F., Fanget, G., Louis, D., Assous, M., Louveau, O., Rivoire, M., Haxaire, K., Mourier, M., Maitrejean, S., Besson, P., Broussous, L., Arnaud, L. and Feldis, H. (2002) Integration of Cu/SiOC in Cu dual damascene interconnect for 0.1-mm technology. *Microelectron. Engng*, **64**, 35–42.

[33] Li, H.Y., Su, Y.J., Tsang, C.F., Sohan, S.M., Bliznetsov, V. and Zhang, L. (2004) Process improvement of 0.13 mm Cu/low *k* (Black Diamond) dual damascene interconnection. *Microelectron. Reliab*., **45**, 1134–1143.

[34] Lin, S., Jin, C., Lui, L., Tsai, M., Daniels, M., Gonzalez, A., Wetzel, J.T., Monnig, K.A., Winebarger, P.A., Jang, S.M., Yu, D. and Liang, M.S. (2001) Low-*k* dielectrics characterization for damscene integration. Proceedings of the 4th IEEE International Interconnect Technology Conference, Burlingame, California, p. 146.

[35] Mosig, K., Jacobs, T., Brennan, K., Rasco, M., Wolf, J. and Augur, R. (2002) Integration challenges of porous ultra low-*k* spin-on dielectrics. *Microelectron. Engng*, **64**, 11–24.

[36] Schwartz, G.C. (2006) Methods/principles of deposition and etching of thin-films, in *Handbook of Semiconductor Interconnection Technology*, 2nd edn (eds Schwartz, G.C. and Srikrishnan, K.V.), CRC Press, Boca Raton, Florida.

[37] Baklanov, M.R., Le, Q.T., Kesters, E., Iacopi, F., van Aelst, J., Struyf, H., Boullart, W., Vanhaelemeersch, S. and Maex, K. (2004) Challenges of clean/strip processing for Cu/low-*k* technology. Proceedings of the 7th IEEE International Interconnect Technology Conference, Burlingame, California, pp. 187–189.

[38] Furukawa, Y., Patz, M., Kokubo, T. and Snijders, J.H.M. (2003) Material modification of the patterned wafer during dry etching and strip determined by XPS. *Microelectron. Engng*, **70**, 267–273.

[39] Furukawa, Y., Wolters, R., Roosen, H., Snijders, J.H.M. and Hoofman, R. (2004) Etch and strip induced material modification of porous low-*k* ($k = 2.2$) dielectric. *Microelectron. Engng*, **76**, 25–31.

[40] Huang, R. (2004) Via fill properties of organic BARCs in dual-damascene application. Proceedings of SPIE – International Society of Optical Engineering, Santa Clara, California, pp. 711–717.

[41] Hussein, M., Sivakumar, S., Brain, R., Beattie, B., Nguyen, P. and Fradkin, M. (2002) A novel approach to dual damascene patterning. Proceedings of the 5th IEEE International Interconnect Technology Conference, Burlingame, California, pp. 18–20.

[42] Lamb, J.E. and Shao, X. (2002) *Fill material for dual damascene processes*, US Patent 6,391,472 B1.

[43] Ryan, E.T., Labelle, C., Nitta, S., Fuller, N.C.M., Bonilla, G., McCullough, K., Taft, C., Lin, H., Simon, A., Simonyi, E., Malone, K., Sankarapandian, M., Dunn, D., Zaitz, M.A., Cohen, S., Klymko, N., Moon, B.K., Li, Z., Li, S., Yan, Y., Liu, J. and Ho, P.S. (2005) Nanoporous materials integration into advanced microprocessors. Proceedings of the Material Research Society Symposium, San Francisco, California, pp. 147–158.

[44] Yang, H.-L., Zhang, F., Nelson, K., Tseng, J.M., Forster, J., Sunddarrajan, A., Bhatnagar, A., Kumar, N. and Gopalraja, P. (2008) Off-angular deposition compensation for PVD selective re-sputtering process. Proceedings of the Material Research Society Symposium, San Francisco, California, Paper 1079-N1003-1005.

[45] Louis, D., Beverina, A., Arvet, C., Lajoinie, E., Peyne, C., Holmes, D. and Maloney, D. (2001) Cleaning status on low-*k* dielectric in advanced VLSI interconnect: characterisation and principal issues. *Microelectron. Engng*, **57–58**, 621–627.

[46] Louis, D., Beverina, A., Arvet, C., Lajoinie, E., Peyne, C., Holmes, D., Maloney, D., Lee, S. and Lee, W.M. (2000) Cleaning process strategies compatible with low-*k* dielectric and copper state of the art, evolution and perspectives. Proceedings of the 3rd IEEE International Interconnect Technology Conference, Burlingame, California, p. 250.

[47] Louis, D., Peyne, C., Lajoinie, E., Vallesi, B., Holmes, D., Maloney, D. and Lee, S. (1999) Improved post etch cleaning for low-*k* and copper integration for 0.18 mm technology. *Microelectron. Engng*, **46**, 307–310.

[48] Iacopi, F., Tokei, Z., Le, Q.T., Shamiryan, D., Conard, T., Brijs, B., Kreissig, U., Van Hove, M. and Maex, K. (2002) Factors affecting an efficient sealing of porous low-*k* dielectrics by physical vapor deposition Ta(N) thin films. *J. Appl. Phys.*, **92**, 1548–1554.
[49] Iacopi, F., Zistl, C., Jehoul, C., Tokei, Z., Le, Q.T., Das, A., Sullivan, C., Prokopowicz, G., Gronbeck, D., Gallagher, M., Calvert, J. and Maex, K. (2002) Dependence of the minimal PVD Ta(N) sealing thickness on the porosity of ZirkonTM LK dielectric films. *Microelectron. Engng*, **64**, 351–360.
[50] Kondo, S., Tokitoh, S., Yoon, B.U., Namiki, A., Sone, A., Ohashi, N., Misawa, K., Sone, S., Shin, H.J., Yoshie, T., Yoneda, K., Shimada, M., Ogawa, S., Matsumoto, I. and Kobayashi, N. (2003) Low-pressure CMP for reliable porous low-*k*/Cu integration. Proceedings of the 6th IEEE International Interconnect Technology Conference, Burlingame, California, pp. 86–88.
[51] Leduc, P., Farjot, T., Savoye, M., Demas, A.-C., Maitrejean, S. and Passemard, G. (2006) Dependence of CMP-induced delamination on number of low-*k* dielectric films stacked. *Microelectron. Engng*, **83**, 2072–2076.
[52] Leduc, P., Farjot, T., Savoye, M., Demas, A.-C., Maitrejean, S. and Passemard, G. (2006) CMP-induced peeling in multi-level ultra low-*k*/Cu interconnects. Proceedings of the Material Research Society Symposium, San Francisco, California, pp. 225–230.
[53] Satyanarayana, S., McGowan, R., White, B. and Hosali, S. (2005) Damage mechanisms in porous low-*k* integration. *Semicond. Int.*, **28**, 63–72.
[54] Brofman, P. (2009) IBM's Packaging Technology Roadmap and the 'collaboratory' approach to advanced packaging development. Proceedings of the International Conference on Electronics Packaging, ICEP 2009, Kyoto, Japan, pp. 1–6.
[55] Dubois, G. (2010) Chip–package interaction from a low-*k* materials perspective. Proceedings of the International Conference on Electronics Packaging, ICEP 2010, Hokkaido, Japan, pp. 448–453.
[56] Gallois-Garreignot, S., Fiori, V. and Nelias, D. (2010) Fracture phenomena induced by front-end/back-end interactions: dedicated failure analysis and numerical developments. *Microelectron. Reliab.*, **50**, 75–85.
[57] Van Driel, W.D. (2007) Facing the challenge of designing for Cu/low-*k* reliability. *Microelectron. Engng*, **47**, 1969–1974.
[58] Susko, R.A., Daubenspeck, T.H., Wassick, T.A., Sullivan, T.D., Sauter, W. and Cincotta, J. (2009) Solder bump electromigration and CPI challenges in low-*k* devices. *ECS Trans.*, **16**, 51–60.
[59] Wang, G., Ho, P.S. and Groothuis, S. (2005) Chip-packaging interaction: a critical concern for Cu/low *k* packaging. *Microelectron. Reliab.*, **45**, 1079–1093.
[60] Uchibori, C.J., Lee, M., Zhang, X., Ho, P.S. and Nakamura, T. (2009) Impact of Cu/low-*k* interconnect design on chip package interaction in flip chip package. Proceedings of Stress-Induced Phenomena in Metallization: 10th International Workshop, Austin, Texas, pp. 185–196.
[61] Liu, X.H., Shaw, T.M., Lane, T.W., Liniger, E.G., Herbst, B.W. and Questad, D.L. (2007) Chip–package-interaction modeling of ultra low-*k*/copper back end of line. Proceedings of the 10th IEEE International Interconnect Technology Conference, Burlingame, California, pp. 13–15.
[62] Appelt, B.K., Chen, W.T. and Lai, Y. (2010) Chip–package interactions at advanced silicon nodes. Proceedings of the International Conference on Electronics Packaging, ICEP 2010, Hokkaido, Japan, pp. 38–42.
[63] Volksen, W., Dubois, G., Kellock, A., Magbitang, T.P., Miller, R.D., Miller, D., Cohen, S., Simonyi, E.E., Ramirez, L., Markle, D., Chen, S., Zhou, S., Wang, X. and Wang, Y. (2008) Mechanical enhancement of low-*k* organosilicates by laser spike annealing. *J. Electrochem. Soc.*, **155**, G224–G230.
[64] Gage, D.M., Peng, L., Stebbins, J., Yim, K.S., Al-Bayati, A., Demos, A. and Dauskardt, R.H. (2010) Effects of e-beam curing on glass structure and mechanical properties of nanoporous organosilicate thin films. *Int. J. Mater. Res.*, **101**, 228–235.
[65] Goto, K., Hashii, S., Matsumoto, M., Miura, N., Furusawa, T., Matsuura, M., Ohsaki, A., Ohara, N., Tsuji, N. and Matsushita, K. (2006) Film characterization and integration of UV-cured ultra low-*k* for 45 nm node Cu/low-*k* interconnects. Proceedings of the Advances in Metals Conference 2005, Colorado Springs, Colorado and Tokyo, Japan, pp. 277–283.

[66] Ito, F., Takeuchi, T. and Hayashi, Y. (2006) Improvement of mechanical properties of porous SiOCH films by post-cure treatments. Proceedings of the Advances in Metals Conference 2005, Colorado Springs, Colorado and Tokyo, Japan, pp. 291–296.
[67] Jousseaume, V., Zenasni, A., Favennec, L., Gerbaud, G., Bardet, M., Simon, J.P. and Humbert, A. (2007) Comparison between E-beam and ultraviolet curing to perform porous a-SiOC:H. *J. Electrochem. Soc.*, **154**, G103–G109.
[68] Nakao, S.-I., Ushio, J., Ohno, T., Hamada, T., Kamigaki, Y., Kato, M., Yoneda, K., Kondo, S. and Kobayashi, N. (2006) UV/EB cure mechanism for porous PECVD/SOD low-*k* SiCOH materials. Proceedings of the IEEE International Interconnect Technology Conference, Burlingame, California, 5–7 June 2006, pp. 66–68.
[69] Yoneda, K., Kato, K., Kondo, S., Kobayashi, N., Matsuki, N., Matsushita, K., Ohara, N., Fukazawa, A. and Kimura, T. (2005) Impacts of UV cure for reliable porous PECVD SiOC integration. Proceedings of the IEEE International Interconnect Technology Conference, Burlingame, California, 5–7 June 2005, pp. 220–222.
[70] Mehta, S., Dimitrakopoulos, C., Augur, R., Gambino, J., Chou, A., Hook, T., Linder, B., Tseng, W., Bolam, R., Harmon, D., Massey, D., Gates, S. and Nye, H. (2006) Evaluation of device damage from e-beam curing of ultra low-*k* BEOL dielectrics. Proceedings of the Advances in Metals Conference 2005, Colorado Springs, Colorado and Tokyo, Japan, pp. 361–367.
[71] Chapelon, L.L., Vitiello, J., Gonchond, J.P., Barbier, D. and Torres, J. (2006) UV curing effects on mechanical and electrical performances of a PECVD non-porogen porous SiOC:H films (in *k* [2.2–2.4] range) for 45 nm node and below. *Microelectron. Engng*, **83**, 2136–2141.
[72] Iacopi, F., Travaly, Y., Eyckens, B., Waldfried, C., Abell, T., Guyer, E.P., Gage, D.M., Dauskardt, R.H., Sajavaara, T., Houthoofd, K., Grobet, P., Jacobs, P. and Maex, K. (2006) Short-ranged structural rearrangement and enhancement of mechanical properties of organosilicate glasses induced by ultraviolet radiation, *J. Appl. Phys.*, **99**, 053511/053511–053511/053517.
[73] Smith, R.S., Tsui, T.Y. and Ho, P.S. (2009) Effects of ultraviolet radiation on ultra-low-dielectric constant thin film fracture properties. *J. Mater. Res.*, **24**, 2795–2801.
[74] Smith, R.S., Tsui, T. and Ho, P.S. (2007) The effect of ultraviolet light curing on the material and fracture properties of a *k*~2.5 low-*k* dielectric. Proceedings of the Materials Research Society Symposium, pp. 27–31.
[75] Marsik, P., Verdonck, P., De Roest, D. and Baklanov, M.R. (2010) Porogen residues detection in optical properties of low-*k* dielectrics cured by ultraviolet radiation. *Thin Solid Films*, **518**, 4266–4272.
[76] Berry, I., Waldfried, C. and Durr, K. (2007) Requirements and constraints on optimizing UV processing of low-*k* dielectrics. Proceedings of the Materials Research Society Symposium, p. B02–01.
[77] Martinez, E., Rochat, N., Guedj, C., Licitra, C., Imbert, G. and Le Friec, Y. (2006) Influence of electron-beam and ultraviolet treatments on low-*k* porous dielectrics. *J. Appl. Phys.*, **100**, 124106/124101–124106/124105.
[78] Kim, T.-S., Tsuji, N., Kemeling, N., Matsushita, K., Chumakov, D., Geisler, H., Zschech, E. and Dauskardt, R.H. (2008) Depth dependence of ultraviolet curing of organosilicate low-*k* thin films. *J. Appl. Phys.*, **103**, 064108/064101–064108/064108.
[79] Kim, T.-S., Tsuji, N., Matsushita, K., Kobayashi, N., Chumakov, D., Geisler, H., Zschech, E. and Dauskardt, R.H. (2008) Tuning depth profiles of organosilicate films with ultraviolet curing. *J. Appl. Phys.*, **104**, 074113/074111–074113/074116.
[80] Gage, D.M., Guyer, E.P., Stebbins, J., Cui, Z., Al-Bayati, A., Demos, A., MacWilliams, K.P. and Dauskardt, R.H. (2006) UV curing effects on glass structure and mechanical properties of organosilicate low-*k* thin films. Proceedings of the IEEE International Interconnect Technology Conference, Burlingame, California, 5–7 June 2006, pp. 149–151.
[81] Gage, D.M., Stebbins, J.F., Peng, L., Cui, Z., Al-Bayati, A., MacWilliams, K.P., M'Saad, H. and Dauskardt, R.H. (2008) Effects of UV cure on glass structure and fracture properties of nanoporous carbon-doped oxide thin films. *J. Appl. Phys.*, **104**, 043513/043511–043513/043518.
[82] Iacopi, F., Beyer, G., Travaly, Y., Waldfried, C., Gage, D.M., Dauskardt, R.H., Houthoofd, K., Jacobs, P., Adriaensens, P., Schulze, K., Schulz, S.E., List, S. and Carlotti, G. (2007) Thermomechanical properties of thin organosilicate glass films treated with ultraviolet-assisted cure. *Acta Mater.*, **55**, 1407–1414.

[83] Kim, T.-S., Chumakov, D., Zschech, E. and Dauskardt, R.H. (2009) Tailoring UV cure depth profiles for optimal mechanical properties of organosilicate thin films. *Appl. Phys. Lett.*, **95**, 071902/071901–071902/071903.

[84] Lin, Y., Xiang, Y., Tsui, T.Y. and Vlassak, J.J. (2008) PECVD low-permittivity organosilicate glass coatings: adhesion, fracture and mechanical properties. *Acta Mater.*, **56**, 4932–4943.

[85] Calvert, J.M. and Gallagher, M.K. (2003) A new approach to ultralow-*k* dielectrics. *Semicond. Int.*, **26**, 56–58, 60.

[86] Dalton, T.J., Greco, S.E., Hedrick, J.C., Nitta, S.V., Purushothaman, S., Rodbell, K.P. and Rosenberg, R. (2002) *Method for forming a porous dielectric layer in a semiconductor device and device formed*, Patent 6,451,712 B1.

[87] Fayolle, M., Jousseaume, V., Assous, M., Tabouret, E., le Cornec, C., Haumesser, P.H., Leduc, P., Feldis, H., Louveau, O., Passemard, G. and Fusalba, F. (2004) Cu/ULK integration using a post integration porogen removal approach. Proceedings of the 7th IEEE International Interconnect Technology Conference, Burlingame, California, pp. 208–210.

[88] Gallagher, M.K. and You, Y. (2002) *Electronic device manufacture*, Patent 6,667,147 B2.

[89] Jousseaume, V., Favennec, L., Zenasni, A. and Passemard, G. (2006) Plasma-enhanced-chemical-vapor-deposited ultralow *k* for a postintegration porogen removal approach. *Appl. Phys. Lett.*, **88**, 182908/182901–182908/182903.

[90] Zielinski, E.M., Russell, S.W., List, R.S., Wilson, A.M., Jin, C., Newton, K.J., Lu, J.P., Hurd, T., Hsu, W.Y., Cordasco, V., Gopikanth, M., Korthuis, V., Lee, W., Cerny, G., Russell, N.M., Smith, P.B., O'Brien, S. and Havemann, R.H. (1997) Damascene integration of copper and ultralow-*k* xerogel for high performance interconnects. Technical Digest – International Electron Devices Meeting, pp. 936–938.

[91] Jin, C., Luttmer, J.D., Smith, D.M. and Ramos, T.A. (1997) Nanoporous silica as an ultralow-*k* dielectric. *MRS Bull.*, **22**, 39–42.

[92] Bonitz, J., Schulz, S.E. and Gessner, T. (2004) Ultra thin CVD TiN layers as diffusion barrier films on porous low-*k* materials. *Microelectron. Engng*, **76**, 82–88.

[93] Furuya, A., Soda, E., Yoneda, K., Yoshie, T., Okamura, H., Shimada, M., Ohtsuka, N. and Ogawa, S. (2004) Pore-sealing by etch-byproduct followed by ALD-Ta adhesion layer for Cu/porous low-*k* interconnects. Proceedings of the 7th IEEE International Interconnect Technology Conference, Burlingame, California, pp. 39–41.

[94] Mourier, T., Jousseaume, V., Fusalba, F., Lecornec, C., Maury, P., Passemard, G., Haumesser, P.H., Maitrejean, S., Cordeau, M., Pantel, R., Pierre, F., Fayolle, M. and Feldis, H. (2003) Porous low *k* pore sealing process study for 65 nm and below technologies. Proceedings of the 6th IEEE International Interconnect Technology Conference, Burlingame, California, pp. 245–247.

[95] Tada, M., Harada, Y., Tamura, T., Inoue, N., Ito, F., Yoshiki, M., Ohtake, H., Narihiro, M., Tagami, M., Ueki, M., Hijioka, K., Abe, M., Takeuchi, T., Saito, S., Onodera, T., Furutake, N., Arai, K., Fujii, K. and Hayashi, Y. (2003) A 65-nm-node, Cu interconnect technology using porous SiOCH film ($k = 2.5$) covered with ultra-thin, low-*k* pore seal ($k = 2.7$). Proceedings of Technical Digest – International Electron Devices Meeting, pp. 845–848.

[96] Abell, T. and Maex, K. (2004) Damage minimized plasma pore sealing of microporous low-*k* dielectrics. *Microelectron. Engng*, **76**, 16–19.

[97] Iacopi, F., Baklanov, M.R., Sleeckx, E., Conard, T., Bender, H., Meynen, H. and Maex, K. (2002) Properties of porous HSQ-based films capped by plasma-enhanced chemical vapor deposition dielectric layers. *J. Vac. Sci. Technol., B*, **20**, 109–115.

[98] White, B., Book, G., Hautala, J. and Tabat, M. (2004) Ultra low-*k* integration solutions using GCIB processing. Proceedings of the 7th IEEE International Interconnect Technology Conferance, Burlingame, California, pp. 193–195.

[99] Wu, Z.C., Lu, Y.C., Chiang, C.C., Chen, M.C., Chen, B.T., Wang, G.J., Chen, Y.T., Huang, J.L., Jang, S.M. and Liang, M.S. (2002) Advanced metal barrier free Cu damascene interconnects with PECVD silicon carbide barriers for 90/65-nm BEOL technology. Technical Digest – International Electron Devices Meeting, pp. 595–598.

[100] Aimadeddine, M., Arnal, V., Roy, D., Farcy, A., David, T., Chevolleau, T., Posseme, N., Vitiello, J., Chapelon, L.L., Guedj, C., Brechet, Y., Volpi, F. and Torres, J. (2006) Effect of CH_4

plasma on porous dielectric modification and pore sealing for advanced interconnect technology nodes. Proceedings of the IEEE International Interconnect Technology Conference, Burlingame, California, pp. 81–83.

[101] Cui, H., Carter, R.J., Moore, D.L., Peng, H.-G., Gidley, D.W. and Burke, P.A. (2005) Impact of reductive N_2/H_2 plasma on porous low-dielectric constant SiCOH thin films. *J. Appl. Phys.*, **97**, 113302/113301–113302/113308.

[102] Arnal, V., Hoofman, R.J.O.M., Assous, M., Bancken, P.H.L., Broekaart, M., Brun, P., Casanova, N., Chapelon, L.L., Chevolleau, T., Cowache, C., Daamen, R., Farcy, A., Fayolle, M., Feldis, H., Furukawa, Y., Goldberg, C., Gosset, L.G., Guedj, C., Haxaire, K., Hinsinger, O., Josse, E., Jullian, S., Louveau, O., Michelon, J., Posseme, N., Rivoire, M., Roman, A., Vandeweyer, T., Verheijden, G.J.A.M. and Torres, J. (2004) Process optimisation and dual damascene integration of porous CVD SiOC dielectric at 2.4 and 2.2 *k*-values for 45 nm CMOS technology. Proceedings of the 7th IEEE International Interconnect Technology Conference, Burlingame, California, pp. 202–204.

[103] Furusawa, T., Machida, S., Ryuzaki, D., Sameshima, K., Ishida, T., Ishikawa, K., Miura, N., Konishi, N., Saito, T. and Yamaguchi, H. (2003) Novel dissoluble hardmask for damage-less Cu/low-*k* interconnect fabrication. Proceedings of the 6th IEEE International Interconnect Technology Conference, San Francisco, California, pp. 195–197.

[104] Hinsinger, O., Fox, R., Sabouret, E., Goldberg, C., Verove, C., Besling, W., Brun, P., Josse, E., Monget, C., Belmont, O., Van Hassel, J., Sharma, B.G., Jacquemin, J.P., Vannier, P.,A. Humbert, A.,D. Bunel, D.,R. Gonella, R.,E. Mastromatteo, E.,D. Reber, D., Farcy, A., Mueller, J., Christie, P., Nguyen, V.H., Cregut, C. and Berger, T. (2004) Demonstration of an extendable and industrial 300 mm BEOL integration for the 65-nm technology node. Technical Digest – International Electron Devices Meeting, pp. 317–320.

[105] Struyf, H., Hendrickx, D., Van Olmen, J., Iacopi, F., Richard, O., Travaly, Y., Van Hove, M., Boullart, W. and Vanhaelemeersch, S. (2005) Low-damage damascene patterning of SiOC(H) low-*k* dielectrics. Proceedings of the IEEE International Interconnect Technology Conference, Burlingame, California, pp. 30–32.

[106] Chang, T.C., Liu, P.T., Shih, F.Y. and Sze, S.M. (1999) Effects of hydrogen on electrical and chemical properties of low-*k* hydrogen silsesquioxane as an intermetal dielectric for nonetchback processes. *Electrochem. Solid-State Lett.*, **2**, 390–392.

[107] Kim, Y.-H., Kim, H.J., Kim, J.Y. and Lee, Y. (2002) Passivation effect on low-*Î*° SiOC dielectrics by H_2 plasma treatment. *J. Korean Phys. Soc.*, **40**, 94–98.

[108] Shieh, J.-M., Tsai, K.-C., Dai, B.-T., Wu, Y.-C. and Wu, Y.-H. (2002) Reduction of etching plasma damage on low dielectric constant fluorinated amorphous carbon films by multiple H_2 plasma treatment. *J. Vac. Sci. Technol., B*, **20**, 1476–1481.

[109] Xu, K., Vereecke, G., Kesters, E., Le, Q.T., Lux, M., Henry, S.A., Kraus, H., Archer, L., Mertens, P.W., Kovacs, F., Dalmer, M., Gaulhofer, E., Luo, S.J., Han, Q.Y. and Berry, I. (2007) Modifications of porous low-*k* by plasma treatments and wet cleaning. *ECS Trans.*, **11**, 409–416.

[110] Grill, A. and Patel, V. (2004) Interaction of hydrogen plasma with extreme low-*k* SiCOH dielectrics. *J. Electrochem. Soc.*, **151**, F133–F134.

[111] Grill, A., Sternhagen, V., Neumayer, D. and Patel, V. (2005) Hydrogen plasma effects on ultralow-*k* porous SiCOH dielectrics. *J. Appl. Phys.*, **98**, 074502/074501–074502/074507.

[112] Berry, I., Shiota, A., Han, Q., Waldfried, C., Sekiguchi, M. and Escorcia, O. (2003) H_2/He plasma for photoresist stripping over porous MSQ low-*k* films. Proceedings of the Electrochem. Society, pp. 202–210.

[113] Bhanap, A., Korolev, B., Nitta, S., Purushothaman, S., Bonilla, G. and Ryan, E.T. (2007) A carbon-restoring silylation process for low-*k* dielectric repair. *Solid State Technol.*, **50**, 79–80, 82, 84, 86.

[114] Mor, Y.S., Chang, T.C., Liu, P.T., Tsai, T.M., Chen, C.W., Yan, S.T., Chu, C.J., Wu, W.F., Pan, F.M., Lur, W. and Sze, S.M. (2002) Effective repair to ultra-low-*k* dielectric material (*k* approx. 2.0) by hexamethyldisilazane treatment. *J. Vac. Sci. Technol., B*, **20**, 1334–1338.

[115] Orozco-Teran, R.A., Gorman, B.P., Mueller, D.W., Baklanov, M.R. and Reidy, R.F. (2004) Effect of silylation on triethoxyfluorosilane xerogel films by means of atmospheric pressure drying. *Thin Solid Films*, **471**, 145–153.

[116] Rajagopalan, T., Lahlouh, B., Chari, I., Othman, M.T., Biswas, N., Toma, D. and Gangopadhyay, S. (2008) Hexamethyldisilazane vapor treatment of plasma damaged nanoporous methylsilsesquioxane films: structural and electrical characteristics. *Thin Solid Films*, **516**, 3399–3404.

[117] Singh, A.P., Gandhi, D.D., Singh, B., Simonyi, E., Liniger, E.G., Nitta, S.V., Lane, M.W. and Ramanath, G. (2009) Pore orientation and silylation effects on mesoporous silica film properties. *Appl. Phys. Lett.*, **94**, 093502/093501–093502/093503.

[118] Chen, J.Y., Pan, F.M., Cho, A.T., Chao, K.J., Tsai, T.G., Wu, B.W., Yang, C.M. and Chang, L. (2003) Microstructure and mechanical properties of surfactant templated nanoporous silica thin films: effect of methylsilylation. *J. Electrochem. Soc.*, **150**, F123–F127.

[119] Liu, J., Kim, W., Bao, J., Shi, H., Baek, W. and Ho, P.S. (2007) Restoration and pore sealing of plasma damaged porous organosilicate low *k* dielectrics with phenyl containing agents. *J. Vac. Sci. Technol., B*, **25**, 906–912.

[120] Jung, J.M., Kwon, H.S., Lee, W.-K., Choi, B.-C., Kim, H.G. and Lim, K.T. (2010) Repair of plasma-damaged p-SiOCH dielectric films in supercritical CO_2. *Microelectron. Engng*, **87**, 1680–1684.

[121] Oszinda, T., Schaller, M. and Schulz, S.E. (2010) Chemical repair of plasma damaged porous ultra low-Î° SiOCH film using a vapor phase process. *ECS Trans.*, **25**, 19–30.

[122] Gorman, B.P., Orozco-Teran, R.A., Zhang, Z., Matz, P.D., Mueller, D.W. and Reidy, R.F. (2004) Rapid repair of plasma ash damage in low-*k* dielectrics using supercritical CO_2. *J. Vac. Sci. Technol., B: Microelectron. Nanometer Struct. – Process., Measmt, Phenom.*, **22**, 1210–1212.

[123] Arakawa, S., Mizuno, I., Ohoka, Y., Nagahata, K., Tabuchi, K., Kanamura, R. and Kadomura, S. (2006) Breakthrough integration of 32 nm-node Cu/ultra low-*k* SiOC ($k = 2.0$) interconnects by using advanced pore-sealing and low-*k* hard mask technologies. Proceedings of the IEEE International Interconnect Technology Conference, Burlingame, California, pp. 210–212.

[124] Usui, T., Tsumura, K., Nasu, H., Hayashi, Y., Minamihaba, G., Toyoda, H., Sawada, H., Ito, S., Miyajima, H., Watanabe, K., Shimada, M., Kojima, A., Uozumi, Y. and Shibata, H. (2006) High performance ultra low-*k* ($k = 2.0/k_{eff} = 2.4$)/Cu dual-damascene interconnect technology with self-formed $MnSi_xO_y$ barrier layer for 32 nm-node. Proceedings of the IEEE International Interconnect Technology Conference, Burlingame, California, pp. 216–218.

[125] Watanabe, T., Hayashi, Y., Tomizawa, H., Usui, T., Gawase, A., Shimada, M., Watanabe, K. and Shibata, H. (2008) Robust BEOL process integration with ultra low-*k* ($k = 2.0$) dielectric and self-formed MnO_x barrier technology for 32 nm-node and beyond. Proceedings of the IEEE International Interconnect Technology Conference, Burlingame, California, pp. 208–210.

[126] Kagawa, Y., Enomoto, Y., Shimayama, T., Kameshima, T., Okamoto, M., Kawashima, H., Yamada, A., Hasegawa, T., Akiyama, K., Masuda, H., Miyajima, H., Shibata, H. and Kadomura, S. (2006) Robust 45-nm node Cu/ULK interconnects using effective porogen control. Proceedings of the IEEE International Interconnect Technology Conf., Burlingame, California, pp. 207–209.

[127] Davis, M.E. and Lobo, R.F. (1992) Zeolite and molecular sieve synthesis. *Chem. Mater.*, **4**, 756–768.

[128] Corma, A. (1997) From microporous to mesoporous molecular sieve materials and their use in catalysis. *Chem. Rev.*, **97**, 2373–2419.

[129] Flanigen, E.M., Bennett, J.M., Grose, R.W., Cohen, J.P., Patton, R.L., Kirchner, R.M. and Smith, J.V. (1978) Silicalite, a new hydrophobic crystalline silica molecular sieve. *Nature (London)*, **271**, 512–516.

[130] Bibby, D.M., Milestone, N.B. and Aldridge, L.P. (1979) Silicalite-2, a silica analog of the aluminosilicate zeolite ZSM-11. *Nature (London)*, **280**, 664–665.

[131] Li, Z., Johnson, M.C., Sun, M., Ryan, E.T., Earl, D.J., Maichen, W., Martin, J.I., Li, S., Lew, C.M., Wang, J., Deem, M.W., Davis, M.E. and Yan, Y. (2006) Mechanical and dielectric properties of pure-silica-zeolite low-*k* materials. *Angew. Chem., Int. Ed.*, **45**, 6329–6332.

[132] Z. Wang, Z.,H. Wang, H.,A. Mitra, A.,L. Huang, L. and Y. Yan, Y. (2001) Pure-silica zeolite low-*k* dielectric thin films. *Adv. Mater.*, **13**, 746–749.

[133] Gaynor, J.F. (2001) *Dielectric layer including silicalite crystals and binder and method for producing same for microelectronic circuits*. Patent 6,329,062.
[134] Gaynor, J.F. (2003) *Dielectric layer including silicalite crystals and binder and method for producing same for microelectronic circuits*. Patent 6,566,243.
[135] Eslava, S., Baklanov, M.R., Kirschhock, C.E.A., Iacopi, F., Aldea, S., Maex, K. and Martens, J.A. (2007) Characterization of a molecular sieve coating using ellipsometric porosimetry. *Langmuir*, **23**, 12811–12816.
[136] Hu, L., Wang, J., Li, Z., Li, S. and Yan, Y. (2006) Interfacial adhesion of nanoporous zeolite thin films. *J. Mater. Res*., **21**, 505–511.
[137] Wang, Z., Mitra, A., Wang, H., Huang, L. and Yan, Y. (2001) Pure silica zeolite films as low-*k* dielectrics by spin-on of nanoparticle suspensions. *Adv. Mater*., **13**, 1463–1466.
[138] Li, S., Sun, J., Li, Z., Peng, H., Gidley, D., Ryan, E.T. and Yan, Y. (2004) Evaluation of pore structure in pure silica zeolite MFI low-*k* thin films using positronium annihilation lifetime spectroscopy. *J. Phys. Chem. B*, **108**, 11689–11692.
[139] Lew, C.M., Liu, Y., Day, B., Kloster, G.M., Tiznado, H., Sun, M., Zaera, F., Wang, J. and Yan, Y. (2009) Hydrofluoric-acid-resistant and hydrophobic pure-silica-zeolite MEL low-dielectric-constant films. *Langmuir*, **25**, 5039–5044.
[140] Li, S., Li, Z. and Yan, Y. (2003) Ultra-low-*k* pure-silica zeolite MFI films using cyclodextrin as porogen. *Adv. Mater*., **15**, 1528–1531.
[141] Li, Z., Li, S., Luo, H. and Yan, Y. (2004) Effects of crystallinity in spin-on pure-silica-zeolite MFI low-dielectric-constant films. *Adv. Funct. Mater*., **14**, 1019–1024.
[142] Li, Z., Lew, C.M., Li, S., Medina, D.I. and Yan, Y. (2005) Pure-silica-zeolite MEL low-*k* films from nanoparticle suspensions. *J. Phys. Chem. B*, **109**, 8652–8658.
[143] Eslava, S., Kirschhock, C.E.A., Aldea, S., Baklanov, M.R., Iacopi, F., Maex, K. and Martens, J.A. (2009) Characterization of spin-on zeolite films prepared from Silicalite-1 nanoparticle suspensions. *Microporous Mesoporous Mater*., **118**, 458–466.
[144] Johnson, M., Li, Z., Wang, J. and Yan, Y. (2007) Mechanical characterization of zeolite low dielectric constant thin films by nanoindentation. *Thin Solid Films*, **515**, 3164–3170.
[145] Eslava, S., Baklanov, M.R., Neimark, A.V., Iacopi, F., Kirschhock, C.E.A., Maex, K. and Martens, J.A. (2008) Evidence of large voids in pure-silica-zeolite low-*k* dielectrics synthesized by spin-on of nanoparticle suspensions. *Adv. Mater*., **20**, 3110–3116.
[146] Davis, T.M., Drews, T.O., Ramanan, H., He, C., Dong, J., Schnablegger, H., Katsoulakis, M.A., Kokkoli, E., McCormick, A.V., Penn, R.L. and Tsapatsis, M. (2006) Mechanistic principles of nanoparticle evolution to zeolite crystals. *Nat. Mater*., **5**, 400–408.
[147] Liu, Y., Sun, M., Lew, C.M., Wang, J. and Yan, Y. (2008) MEL-type pure-silica zeolite nanocrystals prepared by an evaporation-assisted two-stage synthesis method as ultra-low-*k* materials. *Adv. Funct. Mater*., **18**, 1732–1738.
[148] Eslava, S., Seo, J.W., Kirschhock, C.E.A., Baklanov, M.R., Maex, K. and Martens, J.A. (2010) Comment on 'MEL-type pure-silica zeolite nanocrystals prepared by an evaporation-assisted two-stage synthesis method as ultra-low-*k* materials'. *Adv. Funct. Mater*., **20**, 2377–2379.
[149] Liu, Y., Lew, C.M., Sun, M., Cai, R., Wang, J., Kloster, G., Boyanov, B. and Yan, Y. (2009) On-wafer crystallization of ultralow-*k* pure silica zeolite films. *Angew. Chem., Int. Ed*., **48**, 4777–4780, S4777/4771.
[150] Eslava, S., Iacopi, F., Baklanov, M.R., Kirschhock, C.E.A., Maex, K. and Martens, J.A. (2007) Ultraviolet-assisted curing of polycrystalline pure-silica zeolites: hydrophobization, functionalization, and cross-linking of grains. *J. Am. Chem. Soc*., **129**, 9288–9289.
[151] Yoshino, T., Ohnuki, N., Hata, N. and Seino, Y. (2009) Young's modulus enhancement of mesoporous pure-silica-zeolite low-dielectric-constant films by ultraviolet and silylation treatments. *Jpn. J. Appl. Phys*., **48**, 050210/050211–050210/050213.
[152] Li, S., Li, Z., Medina, D., Lew, C. and Yan, Y. (2005) Organic-functionalized pure-silica-zeolite MFI low-*k* films. *Chem. Mater*., **17**, 1851–1854.
[153] Lew, C.M., Li, Z., Li, S., Hwang, S.-J., Liu, Y., Medina, D.I., Sun, M., Wang, J., Davis, M.E. and Yan, Y. (2008) Pure-silica-zeolite MFI and MEL low-dielectric-constant films with fluoro-organic functionalization. *Adv. Funct. Mater*., **18**, 3454–3460.

[154] Zhu, Y., Mueller, T.E. and Lercher, J.A. (2008) Single step preparation of novel hydrophobic composite films for low-*k* applications. *Adv. Funct. Mater.*, **18**, 3427–3433.
[155] Eslava, S., Urrutia, J., Busawon, A.N., Baklanov, M.R., Iacopi, F., Aldea, S., Maex, K., Martens, J.A. and Kirschhock, C.E.A. (2008) Zeolite-inspired low-*k* dielectrics overcoming limitations of zeolite films. *J. Am. Chem. Soc.*, **130**, 17528–17536.
[156] Hobson, S.T. and Shea, K.J. (1997) Bridged bisimide polysilsesquioxane xerogels: new hybrid organic–inorganic materials. *Chem. Mater.*, **9**, 616–623.
[157] Huang, H.H., Orler, B. and Wilkes, G.L. (1985) Ceramers: hybrid materials incorporating polymeric/oligomeric species with inorganic glasses by a sol-gel process. 2. Effect of acid content on the final properties. *Polym. Bull.*, **14**, 557–564.
[158] Huang, H.H., Orler, B. and Wilkes, G.L. (1987) Structure-property behavior of new hybrid materials incorporating oligomeric species into sol-gel glasses. 3. Effect of acid content, tetraethoxysilane content, and molecular weight of poly(dimethylsiloxane). *Macromolecules*, **20**, 1322–1330.
[159] Sharp, K.G. (1998) Inorganic/organic hybrid materials. *Adv. Mater.*, **10**, 1243–1248.
[160] Wen, J. and Wilkes, G.L. (1996) Organic/inorganic hybrid network materials by the sol-gel approach. *Chem. Mater.*, **8**, 1667–1681.
[161] Loy, D.A. and Shea, K.J. (1995) Bridged polysilsesquioxanes. Highly porous hybrid organic–inorganic materials. *Chem. Rev.*, **95**, 1431–1442.
[162] Shea, K.J. and Loy, D.A. (2001) Bridged polysilsesquioxanes. Molecular-engineered hybrid organic–inorganic materials. *Chem. Mater.*, **13**, 3306–3319.
[163] Dubois, G., Magbitang, T., Volksen, W., Simonyi, E. and Miller, R.D. (2005) New spin-on oxycarbosilane low-*k* dielectric materials with exceptional mechanical properties. Proceedings of the IEEE International Interconnect Technology Conference, Burlingame, California, 5–7 June 2005, pp. 226–228.
[164] Dubois, G., Volksen, W., Magbitang, T., Miller, R.D., Gage, D.M. and Dauskardt, R.H. (2007) Molecular network reinforcement of sol-gel glasses. *Adv. Mater.*, **19**, 3989–3994.
[165] Dubois, G., Volksen, W., Magbitang, T., Sherwood, M.H., Miller, R.D., Gage, D.M. and Dauskardt, R.H. (2008) Superior mechanical properties of dense and porous organic/inorganic hybrid thin films. *J. Sol-Gel Sci. Technol.*, **48**, 187–193.
[166] Rathore, J.S., Interrante, L.V. and Dubois, G. (2008) Ultra low-*k* films derived from hyperbranched polycarbosilanes (HBPCS). *Adv. Funct. Mater.*, **18**, 4022–4028.
[167] Choi, B.-G., Kim, B.R., Moon, M.-S., Kang, J.-W. and Ko, M.-J. (2005) New carbon-bridged hybrid polymers for low-*k* materials. *Mater. Res. Soc. Symp. Proc.*, **863**, 121–126.
[168] Char, K., Cha, B.J. and Kim, S. (2004) Material issues for nanoporous ultra low-*k* dielectrics. Proceedings of the 7th IEEE International Interconnect Technology Conference, pp. 219–221.
[169] Kim, B.R., Son, J.M. and Ko, M.J. (2007) The effect of porogen on physical properties in MTMS-BTMSE spin-on organosilicates. *J. Mater. Sci.*, **42**, 5381–5390.
[170] Kim, S., Char, K., Hahn, J., Lee, J.-K., Yoon, D.Y., Rhee, H.-W. and Jin, M.Y. (2007) Effect of pore generating materials on the electrical and mechanical properties of porous low-*k* films. *Macromol. Res.*, **15**, 1–4.
[171] Toivola, Y., Kim, S., Cook, R.F., Char, K., Lee, J.-K., Yoon, D.Y., Rhee, H.-W., Kim, S.Y. and Jin, M.Y. (2004) Organosilicate spin-on glasses. *J. Electrochem. Soc.*, **151**, F45–F53.
[172] Ro, H.W., Char, K., Jeon, E,-c., Kim, H.-J., Kwon, D., Lee, H.-J., Lee, J.-K., Rhee, H.-W., Soles, C.L. and Yoon, D.Y. (2007) High-modulus spin-on organosilicate glasses for nanoporous applications. *Adv. Mater.*, **19**, 705–710.
[173] Hatton, B.D., Landskron, K., Whitnall, W., Perovic, D.D. and Ozin, G.A. (2005) Spin-coated periodic mesoporous organosilica thin films – towards a new generation of low-dielectric-constant materials. *Adv. Funct. Mater.*, **15**, 823–829.
[174] Landskron, K., Hatton, B.D., Perovic, D.D. and Ozin, G.A. (2003) Periodic mesoporous organosilicas containing interconnected $[Si(CH_2)]_3$ rings. *Science*, **302**, 266–269 (2003).
[175] Lu, Y., Fan, H., Doke, N., Loy, D.A., Assink, R.A., LaVan, D.A. and Brinker, C.J. (2000) Evaporation-induced self-assembly of hybrid bridged silsesquioxane film and particulate mesophases with integral organic functionality. *J. Am. Chem. Soc.*, **122**, 5258–5261.

[176] Oliver, M.S., Dubois, G., Sherwood, M., Gage, D.M. and Dauskardt, R.H. (2010) Molecular origins of the mechanical behavior of hybrid glasses. *Adv. Funct. Mater.*, **20**, 2884–2892.

[177] Gates, S.M., Dubois, G., Ryan, E.T., Grill, A., Liu, M. and Gidley, D. (2009) Adjusting the skeleton and pore structure of porous SiCOH dielectrics. *J. Electrochem. Soc.*, **156**, G156–G162.

[178] Gates, S.M., Grill, A., Dimitrakopoulos, C., Patel, V., Chen, S.T., Spooner, T., Ryan, E.T., Cohen, S.A., Simonyi, E., Liniger, E., Ostrovski, Y. and Bhatia, R. (2009) Integration compatible porous SiCOH dielectrics from 45 to 22 nm. Proceedings of the Advances in Metals Conference 2008, pp. 531–536.

[179] Ryan, E.T., Gates, S.M., Grill, A., Molis, S., Flaitz, P., Arnold, J., Sankarapandian, M., Cohen, S.A., Ostrovski, Y. and Dimitrakopoulos, C. (2008) Property modifications of nanoporous pSiCOH dielectrics to enhance resistance to plasma-induced damage. *J. Appl. Phys.*, **104**, 094109/094101–094109/094107.

[180] Frot, T., Volksen, W., Purushothaman, S., Bruce, R.L., and Dubois, G. (2011) Application of the protection/deprotection strategy to the science of porous materials, *Adv. Mater.*, **23**, 2828.